Comenius University in Bratislava

Faculty of Mathematics, Physics and Informatics

BROADBAND APPROACH AS A FRAMEWORK FOR IMPLEMENTATION OF RADIATIVE TRANSFER SCHEME WITH SELECTIVE INTERMITTENCY: COST VERSUS ACCURACY STUDY

Master's Thesis

2015 Bc. Peter Kuma

Comenius University in Bratislava

Faculty of Mathematics, Physics and Informatics

Broadband Approach as a Framework for Implementation of Radiative Transfer Scheme with Selective Intermittency: Cost Versus Accuracy Study

Master's Thesis

Degree Programme: Physics

Field of Study: Meteorology and Climatology

Department: Division of Meteorology and Climatology,
Department of Astronomy, Physics of the Earth and Meteorology

Supervisor: Mgr. Ján Mašek

Bc. Peter Kuma

Bratislava, 2015

Contents

Comenius University in Bratislava Faculty of Mathematics, Physics and Informatics

Broadband Approach as a Framework for Implementation of Radiative Transfer Scheme with Selective Intermittency:

Cost Versus Accuracy Study

Master's Thesis

Degree Programme: Physics Field of Study: Meteorology and Climatology Department: Division of Meteorology and Climatology, Department of Astronomy, Physics of the Earth and Meteorology Supervisor: Mgr. Ján Mašek

Bratislava, 2010

Bc. Peter Kuma

Chapter 1

Introduction

1.1 Radiation Schemes

Radiation schemes (or *radiative transfer codes*) are modules of numerical weather prediction (NWP) models and general circulation models (GCM) responsible for calculation of radiation fluxes in the atmosphere and the ocean. Fluxes are neccessary to quantify diabatic heating of atmospheric or oceanic layers. Radiation schemes contribute significantly to the accuracy of weather prediction, but also take a large fraction of model run time. Therefore, improvements in performance are greatly desired.

Radiation schemes are considered to be a part of model 'physics', i.e. a part of the model parametrising various phenomena not covered by the model dynamical core (implementing the momentum equations).

Chapter 2

Basic Principles of Radiative Transfer

This chapter introduces a number of concepts related to radiative transfer in the Earth's atmosphere, and terms necessary for understanding later chapters unambiguously (as there are many notations in general use). Only the most relevant parts are covered, interested reader is advised to look at Petty (2006), Zdunkowski, Trautmann, and Bott (2007) and Goody and Yung (1995) for a more comprehensive development of the radiative transfer theory.

2.1 The Electromagnetic Spectrum

Radiation in the atmosphere is for the most part well represented by electromagnetic (EM) waves. Electromagnetic waves originate from multiple sources, most importantly the Sun, the Earth's surface and atmospheric gases and continutents (clouds and suspended particles). They have different wavelengths depending on the temperature of the radiating object through the Planck's law. Radiation of different wavelenghts is subject to different levels of absorption and scattering when passing through the atmosphere. Traditionally, the electromagnetic spectrum is split into a number of regions (Fig. **??**):

- Gamma radiation
- X-rays
- Ultraviolet radiation (UV-C, UV-B, UV-A)
- Visible light
- Infrared radiation (near IR, thermal IR, far IR)
- Microwaves
- Radio waves

Not all of them will be of our interset, because they are not represented in the atmosphere in energies high enough to influence its thermal structure. Specifically, our interest will be on everything between UV-C and far infrared.

2.1.1 Ultraviolet Radiation

Ultraviolet radiation (UV) is radiated in appreciable amounts only by very hot objects, such as the Sun. It is highly energetic, capable of causing electrons to be released from atoms (photoionisation) and breaking up molecules (photodissociation). Ultraviolet radiation spans wavelengths 10 – 400 nm. The UV spectrm is further split into multiple subregions, out which only the last three are of interest to atmospheric radiative transmission[1]:

- UV-C: 100 nm–280 nm
- UV-B: 280 nm–320 nm
- UV-A: 320 nm–400 nm

Much of ultraviolet radiation is absorbed high in the atmosphere (stratosphere and mesosphere) by ozone and oxygen, though UV-A reaches the Earth's sufrace with little attenuation. Ultraviolet radiation has to be considered in radiation schemes, because it contributes sigificantly to heating of stratosphere. It is also imporant due to its influence on atmospheric chemistry (Chapman reactions).

2.1.2 Visible Light

The visible part of the spectrum comprises wavelengths which humans can percept with their sight. The likely reason which gave rise to this ability is twofold. (1) This is where the peak power of Sun's radiation is located, and (2) the clear-sky atmosphere is almost transparent in the visible spectrum. Visible light spans the region of about 400 nm–700 nm. In radiation models it has to be considered due to its scattering and absorption by clouds and aerosols, but also due to relatively weak absorption by oxygen and ozone in a number of bands.

2.1.3 Infrared Radiation

Infrared radiation (IR) is emitted by objects of temperatures commonly found on Earth. Infrared spectrum can be split into three additional subregions:

- Near infrared: 700 nm–4.6 μm
- Thermal infrared: 4.6 μm–50 μm
- Far infrared: 50 μm–1 mm

[1]The precise choice of boundaries is somewhat arbitrary, and various definitions can be found.

Radiation in near infrared comes mostly from the Sun, while standard temperature objects emit in the thermal and far infrared. The atmosphere is rather opaque to the infrared radiation. It is absorbed strongly (but not uniformly) by greenhouse gases: water vapour, CO_2, O_3, CH_4, CO, N_2O~ and CFCs, but also by clouds and aerosols. As it is the main means of radiative energy exchange between the surface, atmospheric layers and space, it is of paramount importance to radiation models. Radiation in far infrared approx. above 100 □m gradually ceases to be energetically important due to low power emitted at longer wavelengths.

2.1.4 Shortwave and Longwave Parts of the Spectrum

For the purpose of radiation schemes, it is convenient to adopt two even broader spectral regions – *shortwave* (solar) and *longwave* (thermal) radiation. Though the choice of precise values is arbitrary, we will settle on the following definition:

- Shortwave radiation (UV, visible, near IR): 0–4.6 μm
- Longwave radiation (thermal and far IR) : 4.6 μm–100 μm

The justification for this choice is that the Sun emits radiation mostly between 0.2–4.6 μm, while the Earth's surface and atmosphere emit mostly at wavelengths longer than 4.6 μm, with little overlap between the two (Fig. **??**). As discussed later, this exceptional coincidence allows for decoupling of radiative transfer calculations in the two regions.

2.2 Terms and Definitions

This section summarises terms and definitions of the radiative transfer theory used in later chapters. Especially, there is a number of different notations in use today. We follow those of Petty (2006) due to their clarity for most quantities discussed in this text.

2.2.1 Frequency, Wavelength and Wavenumber

Frequency of a monochromatic EM wave will be denoted $\tilde{\nu}$. Frequency relates to *wavelength* □ via the speed of light $c = \tilde{\nu}\lambda$. Longer wavelengths are sometimes indentified by *wavenumber*[2] $\nu = 1/\lambda$, esp. preferred in the infrared spectrum. It is notable that wavenumbers in cm^{-1} can be conveniently converted to wavelengths in □m by the expression $y = 10000/x$, where x is wavenumber and y wavelength (and vice-versa).

[2] Symbols for frequency and wavenumber are sometimes reversed, with $\tilde{\nu}$ denoting wavenumber, and □ frequency.

2.2.2 Monochromatic Radiance and Radiance

Monochromatic radiance[3] is power transmitted by an electromagnetic wave at certain wavelength passing through a unit surface in a particular direction. Monochromatic radiance depends on wavelength λ, position $\mathbf{r}$ and direction given by a unit vector $\hat{\mathbf{\Omega}}$:

$$I_\lambda = I_\lambda(\mathbf{r}, \hat{\mathbf{\Omega}}) \tag{2.1}$$

Monochromatic radiance has units $\mathrm{Wm}^{-3}\mathrm{sr}^{-1}$. When integrated over an interval of wavelenths, we get *radiance*:

$$I = \int_{\Delta\lambda} I_\lambda \mathrm{d}\lambda = I(\mathbf{r}, \hat{\mathbf{\Omega}}) \tag{2.2}$$

Radiance has units $\mathrm{Wm}^{-2}\mathrm{sr}^{-1}$. As *monochromatic radiance* will be discussed freqently in this text, we will call it simply 'radiance' and denote I and state explicitly if *radiance* is considered by calling it *narrowband* or *broadband radiance*. We will also assume implicit dependence on $\mathbf{r}$ in order to make equations more readable.

2.2.3 Flux Density and Net Flux Density

Flux density is radiance integrated over a hemisphere. In plane parallel geometry, depending on the hemisphere we speak of *upward* or *downward* flux density:

$$F^\uparrow = \int_\uparrow I(\hat{\mathbf{\Omega}}) \mathrm{d}\omega \tag{2.3}$$

$$F^\downarrow = \int_\downarrow I(\hat{\mathbf{\Omega}}) \mathrm{d}\omega \tag{2.4}$$

where $\int_\uparrow$, $\int_\downarrow$ represent integration over the top and bottom hemisphere (resp.).

Net *flux density* is the difference between the upward and downward flux densities:

$$F^{\mathrm{net}} = F^\uparrow - F^\downarrow \tag{2.5}$$

[3] Radiance is sometimes referred to as *intensity*, *irradiance* or *exitance*. The latter two are reserved for radiance incoming on, and emitted from a surface (resp.).

2.2.4 Absorption Coefficient and Cross Section

2.2.5 Emissivity and Albedo

2.2.6 Optical Path and Transmissivity

2.2.7 Heating Rate

Heating rate of a layer of atmosphere by radiation is given by the difference of net flux density between its top and bottom interfaces, which is a consequence of energy conservation – the energy is transferred from radiation to air molecules and airborne particles in the layer.

2.3 The Radiative Transfer Equation

Fundamentally, radiative tranfer is goverened by the Maxwell equations and quantum mechanical principles. However, it is ofen not neccessary to be concerned with the details of the electromagnetic field in the context of energy budget calculations, perhaps with the exception of Mie theory of scattering.

There are three energetically important processes in which radiation interacts with matter in the atmopshere: *scattering*, *absorption* and *emission*. Put together they form the radiative transfer equation.

2.3.1 Scattering

Scattering of radiation occurs when a charged particle is made to oscillate in a passing electromagnetic wave, generating new electromagnetic radiation, which modifies the original field. The is no net exchange of energy between the particle and the field at the end of the process.

We will define the *scattering phase function* to be a function of two unit vectors $\hat{\mathbf{\Omega}}'$ and $\hat{\mathbf{\Omega}}$ (in addition to the implicit dependence on the position $\mathbf{r}$), giving the fraction of radiance scattered from the direction of $\hat{\mathbf{\Omega}}'$ in the of $\hat{\mathbf{\Omega}}$:

$$p = p(\hat{\mathbf{\Omega}}', \hat{\mathbf{\Omega}}) \tag{2.6}$$

subject to normalisation condition (energy conservation):

$$\frac{1}{4\pi} \int_{4\pi} p(\hat{\mathbf{\Omega}}', \hat{\mathbf{\Omega}}) \mathrm{d}\omega = 1 \tag{2.7}$$

In the presence of scattering only, the differential change in radiance is:

$$\mathrm{d}I(\hat{\mathbf{\Omega}}) = -I(\hat{\mathbf{\Omega}})\beta_s \mathrm{d}s + \beta_s \mathrm{d}s \frac{1}{4\pi} \int_{4\pi} p(\hat{\mathbf{\Omega}}', \hat{\mathbf{\Omega}}) I(\hat{\mathbf{\Omega}}') \mathrm{d}\omega' \tag{2.8}$$

i.e. the change in radiance is equal to the amount removed by scattering in all directions, compensated by radiation scattered into the direction of $\hat{\mathbf{\Omega}}$ from all other directions.

2.3.2 Absoprtion

Passing radiation can be absorbed by molecules and particles, whereby the energy of a photon is absorbed to cause an electronic, vibrational or rotational transition (discussed later) in a molecule. This can be later turned into kinetic energy, causing an increase in temperature. The photon is lost in the process, and radiance is reduced by the corresponding amount of energy. The process of absorption follows quantum mechanical principles.

2.3.3 Emission

2.3.4 Beer's Law

2.3.5 Radiative Transfer Equation

The full form of the *radiative transfer equation* (RTE) combines the contributions of extinction, scattering, and emission in a single equation:

$$\begin{aligned} \mathrm{d}I &= -\mathrm{d}I_{\mathrm{ext}} + \mathrm{d}I_{\mathrm{emit}} + \mathrm{d}I_{\mathrm{scat}} \\ \mathrm{d}I(\hat{\mathbf{\Omega}}) &= -\beta_{\mathrm{e}} \mathrm{d}s I(\hat{\mathbf{\Omega}}) + \beta_{\mathrm{a}} \mathrm{d}s B(\hat{\mathbf{\Omega}}) + \beta_{\mathrm{s}} \mathrm{d}s \frac{1}{4\pi} \int_{4\pi} p(\hat{\mathbf{\Omega}}', \hat{\mathbf{\Omega}}) I(\hat{\mathbf{\Omega}}') \hat{\mathbf{n}} \cdot \mathrm{d}\hat{\mathbf{\Omega}}' \end{aligned} \tag{2.9}$$

where $\mathrm{d}s$ is in the direction of $\hat{\mathbf{\Omega}}$.

It is the purpose of radiation schemes to find an approximate solution to the radiative transfer equation. Before this task becomes computationally feasible in operational NWP models, the equation has to be simplified in a number ways, as discussed in the following chapters.

2.4 Solar Constant

The Sun emits radiation which closely matches that of black body of temperature about 5800 K. A fraction of the radiation reaches the top of the atmosphere (ToA). Because of the large distance of Earth from the Sun, the radiation can be considered parallel for most practical purposes. The solar flux density S at ToA in the direction of the Sun varies seasonally with Earth-Sun distance from about 1330 Wm^{-2} in July to 1420 Wm^{-2} in January (in contrast to seasons in the Northern Hemisphere). The solar flux density at mean distance is called *solar constant*, and denoted S_0. Solar constant is ofter cited to have value 1366 Wm^{-2}, though the exact value is time variable. One such variability is associated with the ~11-year solar cycle, but its amplitude is only about 1 Wm^{-2}. Longer-term variability also exists, but it is of little importance to NWP applications.

The solar constant and solar spectrum are best determined from space, where there is unhindered view of the Sun. There have been a number of such satellite-borne measurements performed over the past decades (Liou 2002).

2.5 Scattering on Spherical Particles

Chapter 3

Radiatively Active Gases

Radiation passing through the Earth's atmosphere is modified by the processes of absorption and scattering. Both of the processes are wavelength-dependent, but while scattering can be analysed by Rayleigh scattering, Mie theory and geometric optics, in order to fully grasp absorption we need to be know the specifc absorption lines of radiatively active gases.

Absorption functions of gas molecules can have immensely complicated structure. Figure **??** shows the absorption coefficient of CO_2 in various levels of magnification. Clearly, one needs a very large amount of information to describe the structure fully. As it turns out, smooting the curve by averaging out the details is of little use in calculation of transmittance due to saturation at wavelengths where absorption is strongest (line centers). This will be discussed later, along with shortcuts to handle the situation efficiently.

[CO_2 absorption coefficient.]

3.1 Types of Transitions

Gases absorb and emit radiation radiation at only precise wavelengths[1] due to restrictions imposed by the quantum theory. In particular, the energy has to match of of the allowed *electronic*, *vibrational* or *rotational* transitions.

3.1.1 Electronic Transitions

Electronic transitions are the most energetic, associated with electrons transitioning into other energy levels within atoms, or breaking free entirely, in which case there is a continuum absorption, because any extra energy can transform into kinetic energy

[1] But considering line broadening and continua discussed later in this chapter.

of the escaping electon. Electronic transitions are mostly responsible for absorption in the high-frequency part of the spectrum below 300 nm.

3.1.2 Vibrational Transitions

Vibrational transitions are less energetic than electronic, but more energetic than rotation transitions. They are due to transitions between vibrational modes of multi-atomic molecules. In quantum theory, they can be described by energy levels of a harmonic oscillator, having equally spaced levels obeying the equation

$$E_\nu = h\nu'(\nu + 1/2) \tag{3.1}$$

where □ (Greek 'nu') is the *vibrational quantum number*. Not all molecules are capable of having vibrational transitions. They are subject to the condition that electromagnetic wave has the be able to excert force on the atoms, for which the molecule needs to have a dipole moment (be polarised). Notably, the most abundant atmospheric gas N_2 does not a dipole moments, and therefore does not posses vibrational modes[2]. The number of vibrational modes generally depend on the number of atoms in the molecule.

3.1.3 Rotational Transitions

Rotational transitions are caused transitions between rotational modes of multi-atomic molecules. Rotational modes are quantised by the equation

$$E_J = \frac{1}{2I}L_J^2 = \frac{1}{2I}\left(\hbar\sqrt{J(J+1)}\right)^2 = \frac{\hbar^2}{2I}J(J+1) \tag{3.2}$$

and the corresponding transitions between adjacent modes are

$$\Delta E = E_{J+1} - E_J = \frac{\hbar^2}{2I}\left[(J+1)(J+2) - J(J+1)\right] = \frac{\hbar^2}{I}(J+1) \tag{3.3}$$

where J is the *rotational quantum number* and I is moment of intertia of the molecule. Rotational transitions are the least energetic. As transitions can occur together, and because they are much less energetic than vibrational transitions, they combine to produce vibrational bands with fine structure, centered at a particular wavelength of a vibrational transition.

Not all molecules have rotational transitions. In particular, electromagnetic wave has to be able to exert torque on the molecule. Especially, it needs to have a dipole moment, or an intrinsic magnetic moment (as is the case with O_2).

[2] ALARO cycle 38.

3.2 Shortwave Spectrum

In the shortwave spectrum, absorption takes place mostly in the high-frequency part of the spectrum (Fig. **??**). In particular, gamma radiation, X-rays, UV-C and UV-B are almost entirely absorbed early in their travel through the atmosphere, mostly by oxygen and ozone. As such, and because they consitute only a small contribution of energy to low and mid-altitudes, they are of little concern to us. Above these wavelengths in the visible part of the spectrum, the atmosphere is relatively transparent, with only a few weak bands of ozone and oxygen. In near-infrared, radiation is again absorbed strongly by bands of water vapour and CO_2. This time we have to be concerned, because water vapour is mostly located in the troposphere, where it contributes to heating of atmospheric layers, and the absorption is not flat-out as in very short wave radiation.

3.2.1 O3

Ozone exhibits a number of bands in the shortwave spectrum in three groups: *Hartley bands*, *Huggins bands* and *Chappuis bands* (Figure 3.1]). All of them are in the form of continuum due to photodissociation, although Huggins bands have more irregular structure.

Of the three, Hartley bands are the strongest. They cover the region between 240–310 nm. Because of their strength, they absort most incident solar radiation in the mesopshere and stratosphere.

Huggins bands cover the region of 310–340 nm.

Although Chappuis bands are the weakest of the three, they are important for atomospheric absorption, because they lie in the region of 450–750 nm, where solar radiation is the strongest. Their principal location of absorption is in the troposhpere.

3.2.2 O2

Oxygen absorption happens mostly in the ultraviolet, where it is associated with electronic transitions.

Even thouh O_2 is a homonuclear diatomic molecule with no electic dipole moment, it has a permanent magnetic moment, enabling rotational transitions to occur.

Outside of the ultraviolet region, oxygen absorbs in the *red* and *infra-red* bands. They are associated with the $\mathrm{a} \leftarrow \mathrm{X}$ (resp. $\mathrm{b} \leftarrow \mathrm{X}$) electronic transition in combination with vibrational-rotational transitions. The red bands comprise band A centered at 762 nm, band B at 688 nm, and band □ at 628 nm. Infra-red bands are centered at 1.58 □m, 1.27 □m and 1.06 □m. Although relatively sparse, the red bands are important to the troposheric

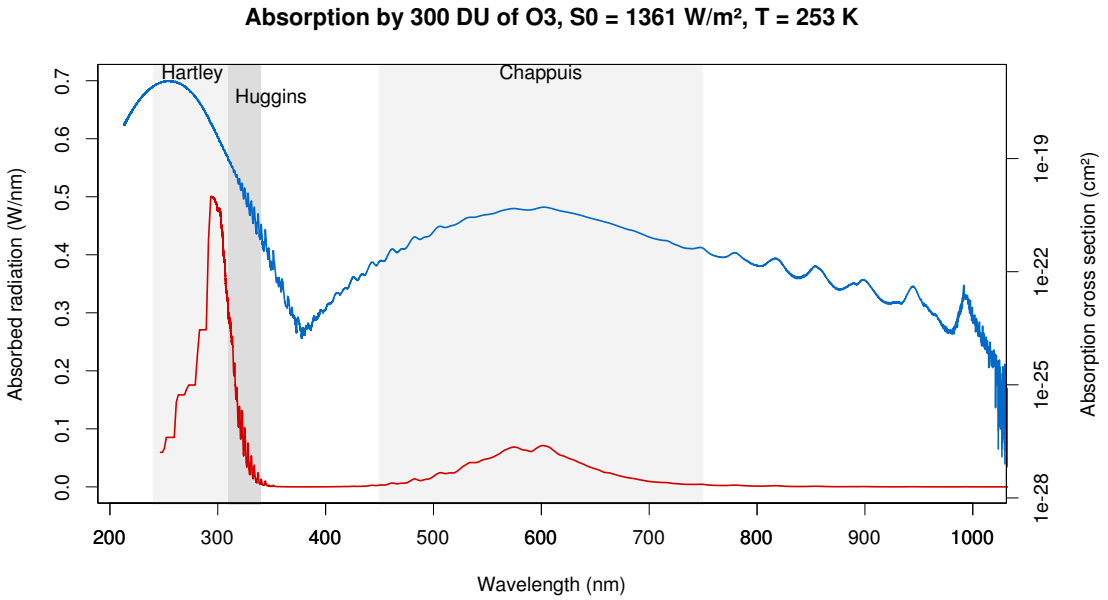

Figure 3.1: Ozone shortwave bands. Absorbed solar radiation (red) and absorption cross section (blue) of O_3. Indicated are approximate regions of the Hartley, Huggins and Chappius absorption bands. Data from Serdyuchenko et al. 2013.

energy budget, because they they are located at the peak of the solar spectrum (Liou 2002).

Oxygen molecules are known to form dimers with some other atmospheric constituents, notably $O_2.N_2$ and O_4. These have additional bands belived to contribute roughly 1 Wm^{-2} to the total atmospheric absorption (Solomon et al. 1998).

3.3 Longwave Spectrum

3.3.1 Water Vapour

3.3.2 CO2

3.3.3 O3

3.3.4 Trace Gases

3.4 Distribution of Gases in the Atmosphere

3.5 Absorption Lines

Atmospheric gases do not in fact absorb and emit radiation at exact wavelengths – if they did we would probably hardly observe any absorption, because the likelihood of an EM wave of exact wavelength interacting with a molecule would be negligible. Instead, absorption lines are spread out over a range of frequencies by three types of processes:

- Natural broadening
- Doppler broadening
- Pressure broadening

Natural broadening occurs due to quantum mechanical effects and is very weak compared to the other two. Therefore, it has little importantce to atmospheric radiative transfer.

Doppler broadening occurs due to Doppler shift in frequency as observed by a moving molecule. It has a normal (Gaussian) shape. Doppler broadening is relative strongest in the upper atmosphere.

Pressure broadening is the most important type of broadening to atmospheric physics. It occurs due to collisions between molecules, which impose a finite time limit on absorption and emission of a monochromatic EM wave.

Effects of all three types of broadening are combined together to produce a characteristic *line shape* of an absorbtion line. Line shape is defined as function f(□), such that:

$$k_\nu = Sf(\nu) \tag{3.4}$$

where S is the strength of a line. The shape function itself is normalised to unity:

$$\int_0^\infty f(\nu)\mathrm{d}\nu = 1 \tag{3.5}$$

3.5.1 Pressure Broadening

Molecules in the atmosphere collide with each other at very high frequency. Every time a collision happens any absorption or emission process which is underway is interrupted. When a stimulation by a monochromatic wave is limited to a finite amount of time, this is equivalent to stimulation by a rage of frequencies, which can be reconstructed by performing Fourier transform on the amplitude function. By taking into account the statistical distribution of time between collisions (Poisson distribution), we can calculate the relative probability of absorpiton/emission at every frequency. The derivation is carried out in e.g. Zdunkowski, Trautmann, and Bott (2007), here we show only the important result – the *Lorentz line shape*:

$$f(\nu) = \frac{\alpha}{\pi[(\nu - \nu_0)^2 + \alpha^2]} \tag{3.6}$$

where $\square_0$ is the line center and $\square$ the line *half-width*. It should be noted that this only applies to high enough wavenumbers (compared to the half-width), but this is only concern to microwaves and longer wavelengths.

The half-width $\square$ depends on the mean time between collision, which can be expressed in terms of pressure and temperature as:

$$\alpha = \alpha_0 \frac{p}{p_0} \left(\frac{T_0}{T}\right)^n \tag{3.7}$$

where $\square_0$ is the half-width at reference pressure and temperature p_0, T_0, and n is empirically determined exponent, which depends on the type of the molecule.

It has to be said that the theory outlined above (*Michelson-Lorentz theory*) does not hold exactly (Goody and Yung 1995). Especially, collisions themselves are not instantaneous, but take finite amount of time. Perhaps most importantly, the Lorentz line shape is insuffiecient in describing the line shape in far-wings of lines, which contribute very significantly to absorption in spectral windows, where there is no other absorption, and a far-wings of many distant lines add up. Overall, it has been established that the Lorentz line shape *underestimates* absorption in far-wings, and *overestimates* absorption near line centers.

3.5.2 Voigt Line Shape

3.5.3 Equivalent Width

The *equivalent width* of a line is the spectral width of a perfectly opaque square line which would absorb the same about of radiation. For a line of any shape it can be calculated as:

$$W = \int_0^\infty (1 - e^{-k_\nu u}) d\nu \tag{3.8}$$

As such, it is not an intrinsic property of a line, but depends on the mass path u.

3.5.4 Weak Line Limit

It is useful to consider the special case when the amount of absorber is relatively small. The equation of equivalent width can then be linearised to give a simplified equation:

$$W = \int_0^\infty (1 - e^{-k_\nu u}) d\nu \approx \int_0^\infty (1 - (1 - k_\nu u)) d\nu = \int_0^\infty S f(\nu) u d\nu = Su \tag{3.9}$$

In the weak line limit, the aborption by a single line is independent from line shape, and it is linear with mass path.

3.5.5 Strong Line Limit

The equivalent width of an arbitrary Lorentz line is:

$$W = \int_0^\infty \left(1 - \exp\left(-\frac{Su\alpha}{\pi[(\nu - \nu_0)^2 + \alpha^2]}\right)\right) d\nu \tag{3.10}$$

If the lower integration limit is extended to -∞, and u is substituted by non-dimensional mass path $\tilde{u} = Su/(2\pi\alpha)$, the integration can be performed analytically to give:

$$W = 2\pi\alpha L(\tilde{u}) \tag{3.11}$$

where L is the Ladenburg-Reiche function, defined in terms of the modified Bessel function of the first kind:

$$L(\tilde{u}) = \tilde{u} e^{-\tilde{u}} [I_0(\tilde{u}) + I_1(\tilde{u})] \tag{3.12}$$

Using this analytical form, it can be shown that for large mass path, equivalent width approaches:

$$W \approx 2\sqrt{S\alpha u} \tag{3.13}$$

This is the *strong line limit*, when absorption by a single line grows in proportion to the square root of mass path $\sqrt{u}$.

The absorption by a single line starts off linearly, but with increasing absorber amount the monochromatic radiance near the line center becomes depleted, and the rate of absorption is reduced to sub-linear (square-root) regime. This can be thought of as *saturation* of absorption, and is similar in the context of multiple overlapping absorption lines.

3.6 Continuum

Gases absorb radiation in discreete absorption lines approximated by the Lorentz or Voigt line shape. However, in some molecules there are parts of the spectrum where the absorption coefficient varies relatively little with wavelength, without apparent association with absorption lines. Typically, this *continuum absoprtion* occurs in connection with photoionization and photodissociation, when the extra energy is consumed by kinetic energy of the escaping electron, resp. broken-up molecules. These processes are mostly confined to the ultraviolet part of the spectrum, because of the high energies requered. In addition to photoionisation and photodissociation, there are other less well- explained sources of continuum absoprtion at lower frequencies due to:

- Far-wings of absorption lines
- *Self continuum*
- *Foreign continuum*
- Absorption by dimers and multimers

Event though contiuum absorption is generally weak comparable to line absorption (with the exception of UV) it is still of great importance, because it convers large parts of the spectrum, often in places where there is absence of line absorption (*atmospheric windows*).

3.6.1 Water Vapour Continuum

Water vapour is the most important source of contiuum for the energy budget, respnsible for as much as 40 % of longwave radiative cooling (Mlawer et al. 2012). The continuum is mostly of two origins: far wings of lines and collision between molecules (self and foreign continuum).

3.6.2 Continua of Other Gases

Chapter 4

Approximate Solutions of the Radiative Transfer Equation

In order to make solution of the radiative transfer equation computationally feasible, and number of approximations are commonly taken in operational radiation schemes.

4.1 Plane Parallel Approximation

The atmopshere forms a thin envelope of the Earth with horizontal scales much pronounced relative to vertical scales. Factors influencing radiative tranfer include gaseous concentrations, clouds, air and surface temperature variation. Perhaps with the exception of cumulus clouds, all of these change slowly in the horizontal direction, and we can simplify the calculations if we treat them as constant over relatively large areas. In NWP models, this is commonly done by dividing the computational domain into a grid and applying *plane parallel approximation* within each grid cell. In plane parallel approximation, the dependence of quantities on (x,y) coordinates is dropped. Quantities are therefore functions of a single spatial coordinate z, or an equivalent vertical coordinate.

Alternative to the plane parallel approximation is a full three-dimensional treatment of radiation, generally performed by Monte Carlo simulation. This is however too computationally expensive to be done in today NWP models.

4.1.1 Layers

In the plane-parallel approximation the atmosphere is often discretised into *layers*, in which quantities such as temperature and gaseous concentrations are constant. Layer interfaces (boundaries) are defined by fixed vertical coordinates, usually pressure levels.

In the following text we assume that layers are numbered from top to bottom by integer number k, where $k = 1$ is the uppermost layer, and $k = N$ the layer just above the surface. Some quantities, such as fluxes, need to be determined on layer interfaces. The layer interface corresponding to the top of the atmopshere will be numered $k = 0$, increasing down to the atmopshere-surface interface $k = N$.

4.1.2 Radiative Transfer Equation in Plane Parallel Approximation

In the plane parallel approximation, the radiative transfer equation can be expressed in terms of a single spatial coordinate z. Defining $\mu \equiv \cos(\theta)$[1] and noting that $\mathrm{d}s = \mathrm{d}z/\mu$, (2.9) transforms to:

$$\mu \frac{\mathrm{d}I(\hat{\mathbf{\Omega}})}{\mathrm{d}z} = -\beta_\mathrm{e} I(\hat{\mathbf{\Omega}}) + \beta_\mathrm{a} B(\hat{\mathbf{\Omega}}) + \frac{\beta_\mathrm{s}}{4\pi} \int_{4\pi} p(\hat{\mathbf{\Omega}}', \hat{\mathbf{\Omega}}) I(\hat{\mathbf{\Omega}}') \mathrm{d}\omega' \tag{4.1}$$

More conveniently, we can use *optical depth* $\mathrm{d}\tau = -\beta_\mathrm{e}\mathrm{d}z$ as a verticalthe vertical coordinate, and normalize by β_e:

$$\mu \frac{\mathrm{d}I(\hat{\mathbf{\Omega}})}{\mathrm{d}\tau} = I(\hat{\mathbf{\Omega}}) - (1-\tilde{\omega}) B(\hat{\mathbf{\Omega}}) - \frac{\tilde{\omega}}{4\pi} \int_{4\pi} p(\hat{\mathbf{\Omega}}', \hat{\mathbf{\Omega}}) I(\hat{\mathbf{\Omega}}') \mathrm{d}\omega' \tag{4.2}$$

where $\tilde{\omega} \equiv \beta_\mathrm{s}/\beta_\mathrm{e}$ is the *single scatter albedo*. This is the *radiative transfer equation in plane parallel atmosphere*.

The geometry of the problem is shown schematically in Figure 6.1.

4.2 Delta-Two Stream Approximation

In the *delta-two stream approximation* radiance is assumed to be constant over hemispheres, with the exception of a forward peak (if present) from direct solar radiation. The forward peak is treated seperately in order to preserve good accuracy, as direct radiation can be orders of magnitude greater than diffuse radiation. There is no azimuthal or zenith dependence of diffuse radiance, and the total radiance is the sum of diffuse and direct radiance:

$$I = I_\mathrm{diff} + I_\mathrm{dir} \tag{4.3}$$

$$I_\mathrm{diff}(\mu, \phi) = \begin{cases} I^\uparrow & \mu > 0 \\ I^\downarrow & \mu < 0 \end{cases} \tag{4.4}$$

[1] As noted by Petty (2006), p. 325, some authors use the definition $\mu_0 \equiv |\cos(\theta)|$. Here, we use $\mu_0 \equiv \cos(\theta)$ as it leads to more straightforward equations in this situtation.

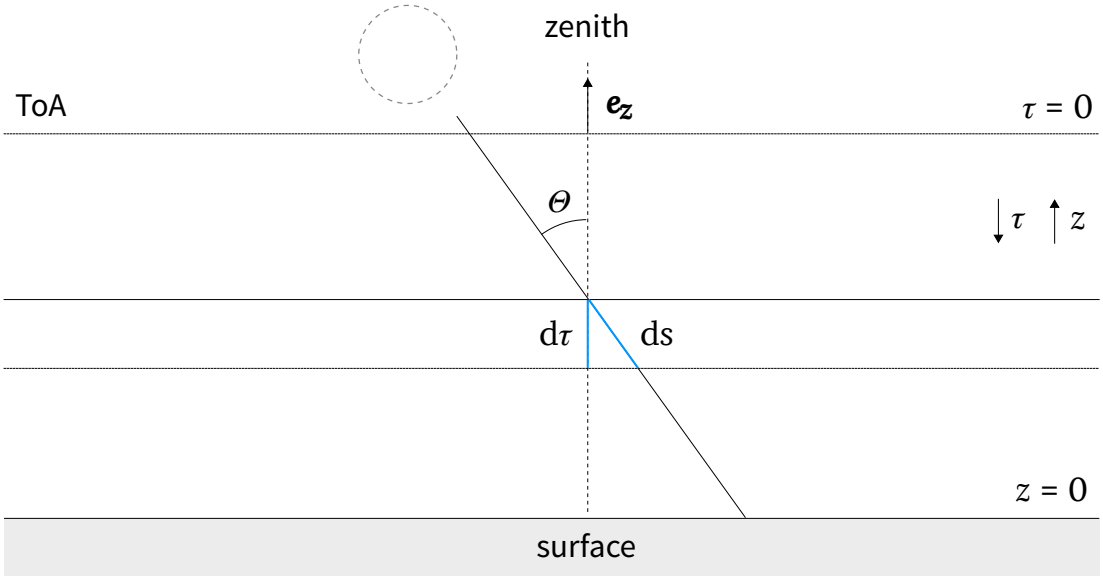

Figure 4.1: Geometry of the plane parallel approximation. Arrows indicate the direction of increase of the optical depth τ and the vertical coordinate z.

where $I^{\uparrow}$ and $I^{\downarrow}$ are upward and downward radiance. $I^{\uparrow}$ and $I^{\downarrow}$ are functions of position only. This allows integration over each hemisphere to be performed analytically to get upward, downward and solar flux density:

$$F^{\uparrow} = \int_{\uparrow} I_{\text{diff}}(\hat{\mathbf{\Omega}})\mathrm{d}\omega = \int_0^{2\pi}\int_0^1 I_{\text{diff}}(\mu,\varphi)\mathrm{d}\mu\mathrm{d}\varphi = 2\pi I^{\uparrow} \tag{4.5}$$

$$F^{\downarrow} = \int_{\downarrow} I_{\text{diff}}(\hat{\mathbf{\Omega}})\mathrm{d}\omega = 2\pi I^{\downarrow} \tag{4.6}$$

$$S = \int_{4\pi} I_{\text{dir}}(\hat{\mathbf{\Omega}})\mathrm{d}\omega \tag{4.7}$$

Therefore, radiance is fully represented by two diffuse flux densities (upward and downward) and flux density of direct (solar) radiation. The upward and downward diffuse flux densities will be denoted as $F_{\uparrow}$ and $F_{\downarrow}$, and flux density of solar radiation as S. Here, we assume that S is coming from the Sun, and so always has a direction somewhere in the bottom hemisphere.

The δ-two stream approximation is justified by the fact that (1) the solar radiation can be orders of magnitude greater that diffuse radiation and (2) the scattering phase function of gases and atmospheric particles tends to be uniform with direction, with the exception of a strong and narrow forward peak.

4.2.1 Radiative Transfer Equation of Direct Radiation

Let us now consider the plane parallel radiative transfer equation (4.2). In our decomposition into diffuse and direct radiation this equation now does not have a unique solution, as I_{diff} and I_{dir} overlap at the angle of the direct radiation, and we cannot tell how much of the value of the right hand side is alloted to the change in diffuse radiation $\mathrm{d}I_{\text{diff}}$ and direct radiation $\mathrm{d}I_{\text{dir}}$ on the left hand side. Therefore, we postulate that the change in direct radiation is only due to extinction of direct radiation and scattering of direct radiation in the direction of the forward δ peak:

$$\mu \frac{\mathrm{d}I_{\text{dir}}(\hat{\mathbf{\Omega}})}{\mathrm{d}\tau} = I_{\text{dir}}(\hat{\mathbf{\Omega}}) - \frac{\tilde{\omega}}{4\pi} \int_{4\pi} p(\hat{\mathbf{\Omega}}', \hat{\mathbf{\Omega}}) I_{\text{dir}}(\hat{\mathbf{\Omega}}') \mathrm{d}\omega', \quad \hat{\mathbf{\Omega}} \in \delta \tag{4.8}$$

To simplify further, we define that the forward peak has the shape of the Dirac δ function[2]:

$$I_{\text{dir}}(\hat{\mathbf{\Omega}}) = S\delta(\hat{\mathbf{\Omega}} \cdot \hat{\mathbf{\Omega}}_0 - 1) \tag{4.9}$$

where $\hat{\mathbf{\Omega}}_0$ is a unit vector in the direction of the radiation, and express the phase function approximately as:

$$p(\hat{\mathbf{\Omega}}', \hat{\mathbf{\Omega}}) \approx (1 - f)p'(\hat{\mathbf{\Omega}}', \hat{\mathbf{\Omega}}) + f\delta(\hat{\mathbf{\Omega}}' \cdot \hat{\mathbf{\Omega}} - 1) \tag{4.10}$$

where $p'(\hat{\mathbf{\Omega}}', \hat{\mathbf{\Omega}})$ is the *δ-scaled phase function*, and f is the fraction scattered in the direction of the forward peak, i.e. we approximate the forward peak by an equivalent Dirac δ peak.

Integrating (4.8) over the δ peak:

$$-\mu_0 \frac{\mathrm{d}S}{\mathrm{d}\tau} = S - \tilde{\omega} f S = S(1 - \tilde{\omega} f) \tag{4.11}$$

where μ_0 is cosine of the zenith angle correspoding to $\hat{\mathbf{\Omega}}_0$: $\mu_0 = -\hat{\mathbf{\Omega}}_0 \cdot \hat{\mathbf{e}}_{\mathbf{z}}$. This motivates us to introduce *delta scaling* $\tau' \equiv \tau(1 - \tilde{\omega} f)$, so that the radiative transfer equation for direct radiation now resembles the Beer's law:

$$\frac{\mathrm{d}S}{\mathrm{d}\tau'} = -\frac{S}{\mu_0} \tag{4.12}$$

[2] It should be noted that the true angle at which radiation passes through a layer depends on the layer height, but here an independent scaling was used. It is also affected by refraction, which is omitted as well.

4.2.2 Radiative Transfer Equations of Diffuse Radiation

In the δ-two stream approximation, the plane parallel radiative transfer equation (4.2) can be integrated analytically over each hemisphere to get a simplified set of differential equations expressed in terms of upward and downward flux density. Integration over the top hemisphere is:

$$\int_{\uparrow} \mu \frac{\mathrm{d}I(\hat{\mathbf{\Omega}})}{\mathrm{d}\tau} \mathrm{d}\omega = \int_{\uparrow} \left[I(\hat{\mathbf{\Omega}}) - (1-\tilde{\omega}) B(\hat{\mathbf{\Omega}}) - \frac{\tilde{\omega}}{4\pi} \int_{4\pi} p(\hat{\mathbf{\Omega}}', \hat{\mathbf{\Omega}}) I(\hat{\mathbf{\Omega}}') \mathrm{d}\omega' \right] \mathrm{d}\omega$$

$$\begin{aligned}
&\frac{1}{2} \frac{\mathrm{d}F^{\uparrow}}{\mathrm{d}\tau} = F^{\uparrow} - (1-\tilde{\omega}) 2\pi B^{\uparrow} - \\
&- \frac{\tilde{\omega}}{4\pi} \left[\int_{\uparrow} \int_{\uparrow} p(\hat{\mathbf{\Omega}}', \hat{\mathbf{\Omega}}) I^{\uparrow} \mathrm{d}\omega' \mathrm{d}\omega + \int_{\uparrow} \int_{\downarrow} p(\hat{\mathbf{\Omega}}', \hat{\mathbf{\Omega}}) I^{\downarrow} \mathrm{d}\omega' \mathrm{d}\omega + \int_{\uparrow} \int_{\downarrow} p(\hat{\mathbf{\Omega}}', \hat{\mathbf{\Omega}}) I_{\mathrm{dir}}(\hat{\mathbf{\Omega}}') \mathrm{d}\omega' \mathrm{d}\omega \right] = \\
&= F^{\uparrow} - (1-\tilde{\omega}) 2\pi B^{\uparrow} - \tilde{\omega} \left[(1-b) F^{\uparrow} + b F^{\downarrow} + \frac{1}{2} b_0 (1-f) S \right]
\end{aligned} \tag{4.13}$$

where we introduced the *backscatter fraction* b and *solar backscatter fraction* b_0:

$$\begin{aligned}
b &\equiv \frac{1}{4\pi} \int_{\uparrow} \int_{\downarrow} p(\hat{\mathbf{\Omega}}', \hat{\mathbf{\Omega}}) I_{\mathrm{diff}}(\hat{\mathbf{\Omega}}') \mathrm{d}\omega' \mathrm{d}\omega \Big/ \int_{\downarrow} I_{\mathrm{diff}}(\hat{\mathbf{\Omega}}') \mathrm{d}\omega' \\
&\equiv \frac{1}{4\pi} \int_{\downarrow} \int_{\uparrow} p(\hat{\mathbf{\Omega}}', \hat{\mathbf{\Omega}}) I_{\mathrm{diff}}(\hat{\mathbf{\Omega}}') \mathrm{d}\omega' \mathrm{d}\omega \Big/ \int_{\uparrow} I_{\mathrm{diff}}(\hat{\mathbf{\Omega}}') \mathrm{d}\omega'
\end{aligned} \tag{4.14}$$

$$b_0 \equiv \frac{1}{4\pi} \int_{\uparrow} \int_{\downarrow} p(\hat{\mathbf{\Omega}}', \hat{\mathbf{\Omega}}) I_{\mathrm{dir}}(\hat{\mathbf{\Omega}}') \mathrm{d}\omega' \mathrm{d}\omega \Big/ \frac{1}{4\pi} \int_{4\pi} \int_{\downarrow} p'(\hat{\mathbf{\Omega}}', \hat{\mathbf{\Omega}}) (1-f) I_{\mathrm{dir}}(\hat{\mathbf{\Omega}}') \mathrm{d}\omega' \mathrm{d}\omega \tag{4.15}$$

which is the fraction of scattered downward radiation scattered upward, and, considering symmetricity of p, it is the same as the fraction of scattered upward radiation scattered downward.

Integration over the bottom hemisphere can be performed analogously to the top hemisphere:

$$\int_{\downarrow} \mu \frac{\mathrm{d}I(\hat{\mathbf{\Omega}})}{\mathrm{d}\tau} \mathrm{d}\omega = \int_{\downarrow} \left[I(\hat{\mathbf{\Omega}}) - (1-\tilde{\omega}) B(\hat{\mathbf{\Omega}}) - \frac{\tilde{\omega}}{4\pi} \int_{4\pi} p(\hat{\mathbf{\Omega}}', \hat{\mathbf{\Omega}}) I(\hat{\mathbf{\Omega}}') \mathrm{d}\omega' \right] \mathrm{d}\omega$$

$$\frac{1}{2}\frac{\mathrm{d}F^{\downarrow}}{\mathrm{d}\tau}+\mu_0\frac{\mathrm{d}S}{\mathrm{d}\tau}=F^{\downarrow}+S-(1-\tilde{\omega})2\pi B^{\downarrow}-$$
$$-\frac{\tilde{\omega}}{4\pi}\left[\int_{\downarrow}\int_{\uparrow}p(\hat{\mathbf{\Omega}}',\hat{\mathbf{\Omega}})I^{\uparrow}\mathrm{d}\omega'\mathrm{d}\omega+\int_{\downarrow}\int_{\downarrow}p(\hat{\mathbf{\Omega}}',\hat{\mathbf{\Omega}})I^{\downarrow}\mathrm{d}\omega'\mathrm{d}\omega+\int_{\downarrow}\int_{\downarrow}p(\hat{\mathbf{\Omega}}',\hat{\mathbf{\Omega}})I_{\mathrm{dir}}(\hat{\mathbf{\Omega}}')\mathrm{d}\omega'\mathrm{d}\omega\right]=$$
$$=F^{\downarrow}+S-(1-\tilde{\omega})2\pi B^{\downarrow}-\tilde{\omega}\left[(1-b)F^{\downarrow}+bF^{\uparrow}+\frac{1}{2}(1-b_0)(1-f)S+fS\right] \tag{4.16}$$

from which we can subtract the equation for direct radiation (4.11) to get:

$$\frac{1}{2}\frac{\mathrm{d}F^{\downarrow}}{\mathrm{d}\tau}=F^{\downarrow}-(1-\tilde{\omega})2\pi B^{\downarrow}-\tilde{\omega}\left[(1-b)F^{\downarrow}+bF^{\uparrow}+\frac{1}{2}(1-b_0)(1-f)S\right] \tag{4.17}$$

4.2.3 Delta Scaling

Putting together the derived equations from the previous two sections (4.12), (**??**), (4.17), the final radiative transfer equations in the δ-two stream approximation are:

$$\frac{1}{2}\frac{\mathrm{d}F^{\uparrow}}{\mathrm{d}\tau}=F^{\uparrow}-(1-\tilde{\omega})2\pi B^{\uparrow}-\tilde{\omega}(1-b)F^{\uparrow}-\tilde{\omega}bF^{\downarrow}-\tilde{\omega}b_0(1-f)\frac{S}{2\mu_0} \tag{4.18}$$
$$-\frac{1}{2}\frac{\mathrm{d}F^{\downarrow}}{\mathrm{d}\tau}=F^{\downarrow}-(1-\tilde{\omega})2\pi B^{\downarrow}-\tilde{\omega}(1-b)F^{\downarrow}-\tilde{\omega}bF^{\uparrow}+\tilde{\omega}(1-b_0)(1-f)\frac{S}{2\mu_0} \tag{4.19}$$
$$\frac{\mathrm{d}S}{\mathrm{d}\tau'}=-\frac{S}{\mu_0} \tag{4.20}$$

We can apply the delta scaling $\tau'=\tau(1-\tilde{\omega}f)$ to the upward and downward flux equations in addition to the direct radiation, and maintain the same structure of the equations by a suitable scaling of $\tilde{\omega}$ and b:

$$\tilde{\omega}'=\tilde{\omega}\left[\frac{1-f}{1-f\tilde{\omega}}\right] \tag{4.21}$$
$$b'=b\left[\frac{1}{1-f}\right] \tag{4.22}$$
$$b_0'=b_0 \tag{4.23}$$

after which the equations for diffuse radiation become:

$$\frac{1}{2}\frac{\mathrm{d}F^{\uparrow}}{\mathrm{d}\tau'} = F^{\uparrow} - (1-\tilde{\omega}')2\pi B^{\uparrow} - \tilde{\omega}'(1-b')F^{\uparrow} - \tilde{\omega}'b'F^{\downarrow} - \tilde{\omega}'b'_0\frac{S}{2\mu_0} \tag{4.24}$$

$$-\frac{1}{2}\frac{\mathrm{d}F^{\downarrow}}{\mathrm{d}\tau'} = F^{\downarrow} - (1-\tilde{\omega}')2\pi B^{\downarrow} - \tilde{\omega}'(1-b')F^{\downarrow} - \tilde{\omega}'b'F^{\uparrow} + \tilde{\omega}'(1-b'_0)\frac{S}{2\mu_0} \tag{4.25}$$

4.2.4 Differential Form of the Radiative Transfer Equation

More concisely, these can be expressed using *differential layer coefficients* α_1, ..., α_4:

$$\frac{\mathrm{d}F^{\uparrow}}{\mathrm{d}\tau} = \alpha_1 F^{\uparrow} - \alpha_2 F^{\downarrow} - \alpha_3\frac{S}{\mu_0} - (\alpha_1-\alpha_2)\pi B \tag{4.26}$$

$$\frac{\mathrm{d}F^{\downarrow}}{\mathrm{d}\tau} = \alpha_2 F^{\uparrow} - \alpha_1 F^{\downarrow} + \alpha_4\frac{S}{\mu_0} + (\alpha_1-\alpha_2)\pi B \tag{4.27}$$

$$\frac{\mathrm{d}S}{\mathrm{d}\tau} = -\frac{S}{\mu_0} \tag{4.28}$$

where:

- $\alpha_1 = 2(1-\tilde{\omega}(1-b))$ is diffuse transmissivity,
- $\alpha_2 = 2b\tilde{\omega}$ is diffuse reflectivity,
- $\alpha_3 = b_0\tilde{\omega}$ is solar to diffuse backscattering,
- $\alpha_4 = (1-b_0)\tilde{\omega}$ is solar to diffuse forward scattering.

This system of equations simplifies in both shortwave and longwave parts of the spectrum: in shortwave $B = 0$, in longwave $S = 0$.

4.2.5 Integral Form of the Radiative Transfer Equation

The coupled system of linear ordinary differential equations (4.26)–(4.28) can be solved for a homogeneous layer by diagonalisation and subsequent integration. While straightforward, the solution is complicated to perform, and we list only the result here according to J Mašek et al. (2014). Also see e.g. Zdunkowski, Trautmann, and Bott (2007), Sec. 6.4 for a worked out solution.

Integrated over a layer from τ_t (top) to τ_b (bottom), the diffuse and direct fluxes have the following linear relationship:

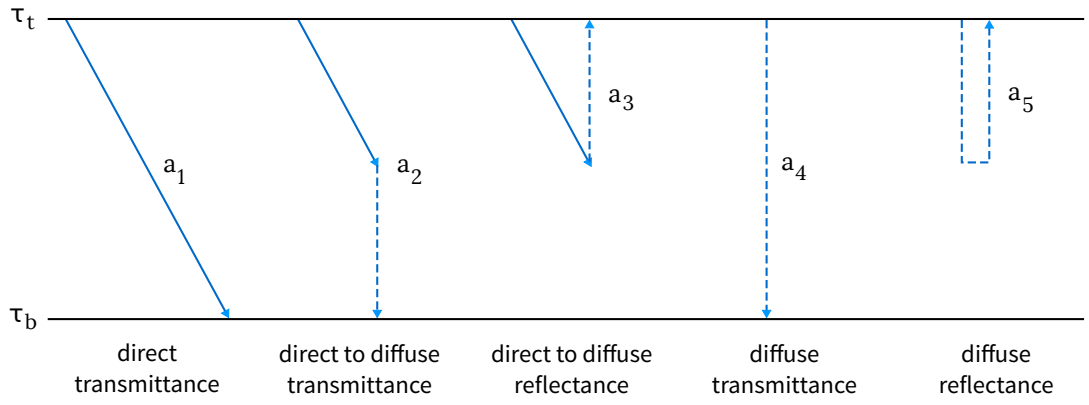

Figure 4.2: Schematic view of the integral layer coefficients. Full lines indicate direct radiation, dashed lines indicate diffuse radiation passing through an atmospheric layer bounded by optical depths τ_t and τ_b.

$$\begin{bmatrix} S(\tau_b) \\ F^{\downarrow}(\tau_b) \\ F^{\uparrow}(\tau_t) \end{bmatrix} = \begin{bmatrix} a_1 & 0 & 0 \\ a_2 & a_4 & a_5 \\ a_3 & a_5 & a_4 \end{bmatrix} \begin{bmatrix} S(\tau_t) \\ F^{\downarrow}(\tau_t) \\ F^{\uparrow}(\tau_b) \end{bmatrix} \tag{4.29}$$

where the *integral layer coefficients* a_1, ..., a_5 can be interpreted as:

- a_1: *direct transmittance*
- a_2: *direct to diffuse transmittance*
- a_3: *direct to diffuse reflectance*
- a_4: *diffuse transmittance*
- a_5: *diffuse reflectance*

The meaning of the coefficients is shown schematically in Figure 4.2.

4.2.6 Diffusivity Factor

In the simple application of two stream approximation, we assume that diffuse radiation is hemispherically isotropic at all points along the vertical axis z. When integrating verticaly over a finite path (a slab of atmosphere), however, we can improve the accuracy if we take into consideration that within the slab radiance may have full directional dependence and preserve hemispheric isotrophy on the boundaries only. This allows us to account for the fact that radiation traversing the slab at different angles passes through different path lengths, and thus is subject to different levels of attenuation.

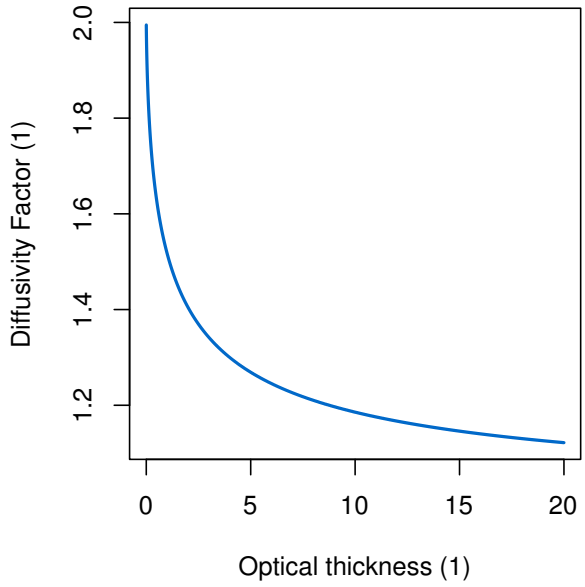

Figure 4.3: Dependence of monochromatic diffusivity factor on optical thickness. Diffusivity factor ranges from 2 for very small optical thickness to 1 for large optical thickness.

It is possible to introduce a single parameter U, called *diffusivity factor*, into the integral form of the radiative transfer equation to rescale the optical depth, and improve its accuracy significantly.

First, we consider the case of simple Beer's law, i.e. without scattering. In the two stream approximation:

$$\mu \frac{\mathrm{d}I}{\mathrm{d}\tau} = -I \quad / \int_{\downarrow} (...) \mathrm{d}\omega \tag{4.30}$$

$$\frac{1}{2} \frac{\mathrm{d}F_{\downarrow}}{\mathrm{d}\tau} = -F_{\downarrow} \tag{4.31}$$

$$F_{\downarrow}(\tau) = F_{\downarrow}(0) \exp(-2\tau) \tag{4.32}$$

However, the true $F_{\downarrow}(\tau)$ is:

$$F_{\downarrow}(\tau) = \int_{\downarrow} I(\tau) \mathrm{d}\omega = \int_{\downarrow} \int_{0}^{\tau} I(0) \exp(-\tau') \mathrm{d}\tau' \mathrm{d}\omega \tag{4.33}$$

If we instead introduce a more flexible form of (4.32) with the diffusivity factor:

$$F_{\downarrow}(\tau) = F_{\downarrow}(0) \exp(-U\tau) \tag{4.34}$$

and require that such $F_{\downarrow}(\tau)$ is the exact flux as in (4.33), we can solve for $U(\tau)$ to get a curve as in Figure 4.3. The values range from 2 for $\tau \ll 1$ (*no scaling* relative to unmodified two stream approximation) to 1 for $\tau \gg 1$.

The situation is more complicated if we consider broadband radiation, where optical satuation modifies the level of attenuation with respect to monochromatic radiation in a path-dependent way. Generally, a single value of U between 1 and 2 is chosen in radiation schemes, such that good practical results are obtained.

4.3 Band Models

Radiatively active gases usually have many more absorption lines than can be integrated over in NWP models in a time-effective manner. A number of statistical approaches to this problem have been invented. One well-established approach is *band models*, whereby line strengths are given by a statistical distribution specified by a limited number of parameters in each band (range of walengths). For suitably chosen distributions, the integration can be done analytically, leading to an expression for broadband transmissivity as a function of path length and distribution parameters. Traditionally, the band size has to be small enough that radiant power (Planck function) can be assumed constant within the band. With some effort this restriction can be lifted, at the cost of more complicating matters such as secondary saturation.

4.3.1 Malkmus Model

One of the most popular *narrow-band* models is the *Malkmus model*. It is based on the assumption that there is a given number of randomly distributed absorption lines in each band, and their stength has probability density:

$$p(S) = \frac{1}{S} e^{-S/S_0} \tag{4.35}$$

where $S_0 = \int_0^\infty S p(S) dS$ is the mean line strength.

Optical depth at wavenumber ν is the sum of contributions of all lines:

$$\tau = ku = \sum_{n=0}^{N} S_i u f(\nu) = \sum_{n=0}^{N} \frac{S_i u \alpha}{\pi[(\nu - \nu_i)^2 + \alpha^2]} \tag{4.36}$$

where $f(\nu)$ is the Voigt line shape, and narrow-band transmissivity

$$\mathcal{T} = \frac{1}{\Delta\nu} \int_{\nu_1}^{\nu_2} e^{-\tau} d\nu = \frac{1}{\Delta\nu} \int_{\nu_1}^{\nu_2} \exp\left(- \sum_{n=0}^{N} \frac{S_i u \alpha}{\pi[(\nu - \nu_i)^2 + \alpha^2]} \right) d\nu \tag{4.37}$$

The above expression is a random variable (because S_i and ν_i are random variables). Therefore, we have to compute mean transmissivity to be useful:

$$\bar{\mathcal{T}} = \int_{\mathbf{S}} \int_{\nu} \mathcal{T} p(\nu) p(\mathbf{S}) d\nu d\mathbf{S} \tag{4.38}$$

where $\mathbf{S} = (S_1, ..., S_N)$ and $\nu = (\nu_1, ..., \nu_N)$ are vectors of line strengths and line positions. This integration can be performed analytically (see e.g. Zdunkowski, Trautmann, and Bott 2007), leading to the *Malkmus formula* for optical depth:

$$\tau_M = \frac{\pi\alpha}{2\delta}\left(\sqrt{1 + \frac{4\bar{S}u}{\pi\alpha}} - 1\right) \tag{4.39}$$

where δ is the average line spacing. This formula can be adapted to the case of non-uniform line width α by comparing two limiting cases of small and large mass paths to the weak and strong line limits derived in Sec. ?. The formula is first written in terms of two parameters a and b:

$$\tau_M = \frac{a}{2b}\left(\sqrt{1 + 4bu} - 1\right) \tag{4.40}$$

By making approximations for $4bu \ll 1$ and $4bu \gg 1$ match the weak and strong line limits, one can show that:

$$a = \sum S_i \tag{4.41}$$

$$b = a^2 / \left(\sum 2\sqrt{S_i \alpha_i)}\right)^2 \tag{4.42}$$

4.3.2 Optical saturation

From the equation for Malkmus model (4.40) we can see that the increase of optical depth with absorber amount u is nonlinear. This phenomenon is sometimes called *optical saturation*, i.e. absorption by an absorption line can contribute to narrow band optical depth only until substantial fraction of radiation at the wavelength is depleted. After that, the radiation no longer contains certain wavelengths and optical depth increases more slowly. This is in contrast with monochromatic absorption and gray broadband absorption, when optical depth increases linearly with absorber amount at all times (Figure 4.4).

We should note that the asymptotic behaviour of the narrow band Malkmus model is:

- $\tau \propto u$ for relatively small absorber amount (weak limit)

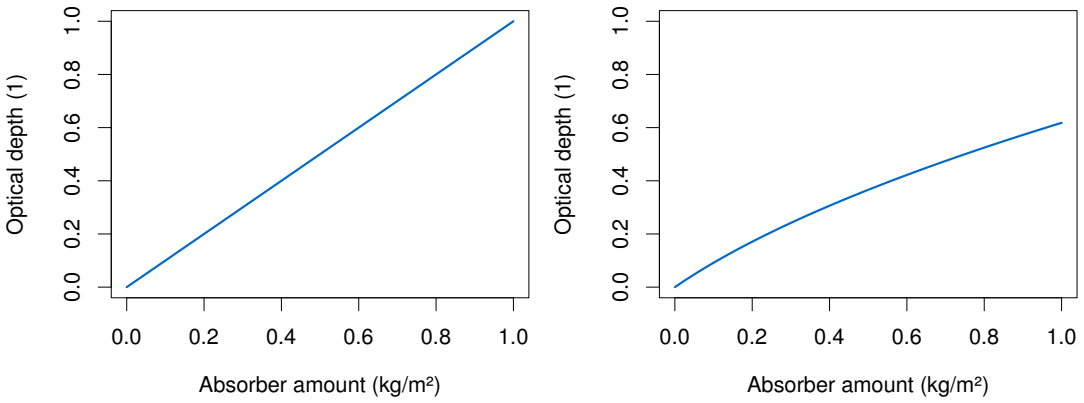

Figure 4.4: Monochromatic and narrow band optical depth. In the monochromatic case (**left**), the increase in optical depth is linear, whereas in a narrow band model (**right**) optical saturation causes increase to be progressively more sublinear. Shown is a Malkmus model as in (4.40).

- $\tau \propto \sqrt{u}$ for relatively large absorber amount (strong limit)

When considering optical depth of larger spectral intervals (where narrow band approximation no longer applies), we can observe *secondary saturation*, when diminising rate of optical depth increase is caused by variability of extinction with wavelength such as in Rayleigh scattering, and in cloud absorption and scattering. While this is not an issue to narrow band model radiation schemes, it has to be taken into account in broadband model radiation schemes *in addition* to optical saturation.

4.3.3 Curtis-Godson Approximation

The Malkmus formula has a number of drawbacks. One of the more serious is that the line width □ is assumed to be constant over the path. In reality, we often need to compute transmissivity over large parts of the atmosphere, where □ varies with pressure and temperature due to line broadening. This situation is handled by the *Curtis-Godson approximation* for inhomogeous atmospheres.

4.4 k-distribution Method

4.5 Continuum

4.5.1 MT_CKD

One of the most comprehensive model of continuum absorption is MT_CKD produced by AER (Mlawer et al. 2012). It includes continuum absorption by water vapor, nitrogen, oxygen, carbon dioxide and ozone. The model uses a semi-empirical approach in which theoretical imact line shape modified by a □-function is fitted by measured values.

4.6 Adding Method

The *adding method* is a method of finding a solution to fluxes for given optical depths and temperature of layers. The adding method assumes that the plane parallel approximation, □-two stream approximation and layer discretisation have been made.

A relationship between fluxes at the top and bottom interfaces of a layer can be found from the □-two-stream differential equations.

$$\begin{pmatrix} S_k \\ F_k^{\downarrow} \\ F_{k-1}^{\uparrow} \end{pmatrix} = \begin{pmatrix} a_1 & 0 & 0 \\ a_2 & a_3 & a_4 \\ a_5 & a_6 & a_7 \end{pmatrix} \begin{pmatrix} S_{k-1} \\ F_{k-1}^{\downarrow} \\ F_k^{\uparrow} \end{pmatrix} \tag{4.43}$$

The equations for all layers can be consolidated into a system of linear equations:

$$\mathbb{A}\mathbf{F} = \mathbf{S} \tag{4.44}$$

where $\mathbb{A}$ is a matrix of coefficients (layer transmissivities and reflectivities), $\mathbf{F}$ is a vector of fluxes and $\mathbf{S}$ is a vector of sources. This system can then be solved for $\mathbf{F}$, which is the desired outcome of the adding method.

4.7 Net Exchange Rate Formulation

4.8 Computational Intermittence

Because the temporal variability of all quantities coming as an input to the RTE is not the same, it is convenient to avoid repeated computation of certain results. E.g., the rate of change of cloudiness is much higher than that of gas concentrations. Therefore, it

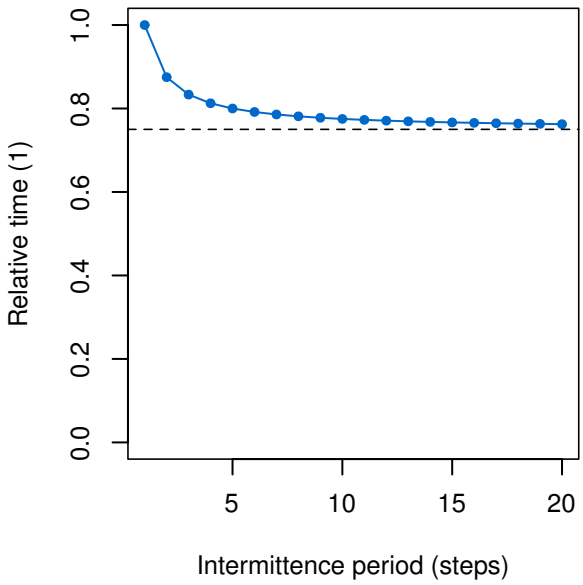

Figure 4.5: Relative model run time with computational intermittence. The relative run time decreases at a diminishing rate as the intermittence period increases, eventually converging to a constant. In this example, a full step time fraction $q = 0.5$, and intermittent step time fraction $q' = 0.5q$ are assumed.

is possible skip or linearise the computation of gaseous transmission functions. Other intermediate results may also be reused, depending on the actual implementation of the solution.

4.8.1 Diminising Performance Gain of Computational Intermittence

Computational intermittence allows us to reduce the computation time of intermittent steps when approximate results are calculated (e.g. by interpolation), while full steps take an unchanged amount of time (or somewhat greater, depending on implementation details). Radiation schemes constitute a fraction of total run time of an NWP model, typically 20–60 % (?). Therefore, there is a limit on the total time reduction due to performance improvements in the radiation scheme alone. Moreover, as we increase the length of the intermittence period (the number of intermittent steps per the number of full steps), there is a diminishing improvement in total run time, to the point that intermittent steps far outnumber full steps, and the computation time of full steps ceases to matter. The accuracy will continue to decrease, however.

Let us assume that a model time step takes time t_m to compute, and the model initialisation/deinitialisation time is t_0. The total model run time when n steps are computed is then:

$$t(n) = t_0 + t_m n \tag{4.45}$$

If a full step of our module (radiation scheme) takes a fraction q of the model time step to compute, and an intermittent step takes $q' < q$, and we choose intermittence period of k steps, the total model run time will be:

$$t'_k(n) = t_0 + t_m q \frac{n}{k} + t_m q' \left(n - \frac{n}{k} \right) + t_m (1 - q) n \tag{4.46}$$

i.e. the sum of initialisation time, time of full steps, time of intermittent steps, and the rest of the model. The relative model run time will be:

$$\tau_k = \frac{t'_k(n)}{t(n)} \approx 1 - (q - q') \left(1 - \frac{1}{k} \right) = 1 - q \left(1 - \frac{q'}{q} \right) \left(1 - \frac{1}{k} \right) \tag{4.47}$$

where we neglected the initialisation time ($t_0 \ll t(n)$). Therefore, when $k \to \infty$, $\tau_k \to 1 - (q - q')$, and there is a diminishing gain in performance as k increases.

Figure 4.5 demonstrates τ_k for a particular choice of parameters. We can see that considering improvement in the total model run time is important when deciding the lenght of the intermittence period, especially considering the detrimental effect intermittence might have the result accuracy.

Chapter 5

Overview of the Radiation Scheme ACRANEB2

ACRANEB (J. Geleyn and Hollingsworth 1979; Ritter and J.-F. Geleyn 1992; J. Geleyn, Fournier, et al. 2005; J Mašek et al. 2014) is a broadband radiation scheme developed as an alternative to k-distribution radiation schemes. k-distribution schemes are currently the most popular method of solving the radiative transfer equation in NWP models, thanks to their superior properties to narrow band models used previously. Their computation complexity, however, precludes frequent recalculation of fluxes due to changing cloudiness. The bradband approach in ACRANEB allows for computational intermittency and decoupling of quickly changing cloudiness from slowly changing gaseous absorption in radiative computations. As a result, the radiative code can be called at every time step, responding rapidly to the development of cloud cover.

We can characterise the scheme by the choices of methods and approximations:

- horizontally homogeneous
- δ-two stream approximation
- broadband model based (two bands: shortwave and longwave)
- adding method for flux computation

ACRANEB2 is currently used operatively in the NWP model ALADIN/ALARO of the RC LACE[1] community. Work on version 2 of ACRANEB commenced in 2011, and this text incorporates the recent developments.

5.1 Operation Overview

The ACRANEB scheme is run on a single cell of the model computational grid. Vertically, the atmosphere is split into layers, on which the computation is discretizated. In the ALARO model, the layers are defined in hybrid *eta cooridates*, transitioning smoothly

[1] Regional Cooperation for Limited Area modeling in Central Europe.

from □-coordinates near the surface to pressure coordinates in the free atmosphere. Therefore, boundary layers follow the ground, while upper layers follow isobaric surfaces.

Apart from an NWP model, ACRANEB can be run in isolation inside a single-cell model. This is useful mostly for diagnostic purposes.

5.1.1 Input and output

The input to the radiation scheme consists of:

- Pressure profile
- Temperature profile
- Concentration of gases
- Cloud fraction and cloud water/ice content
- Aerosol fraction and properties
- Surface temperature and albedo/emissivity
- Solar constant

The output of the scheme are broadband fluxes at layer interfaces, from which the heating rate of layers can be calculated by the rest of the NWP model.

5.1.2 General principle of operation

The general operation of the scheme can be summarised as follows:

1. Optical thickness and transmissivity/reflectivity coefficients of layers are calculated. These are due to gases, clouds and aerosols. The resulting layer coefficients are a weighted sum of layer coefficients for the particular processes, weighted by optical thickness (J Mašek et al. 2014):

$$\alpha_i = \frac{1}{\Delta\delta} \sum_j \alpha_{i,j} \Delta\delta_j, \quad \Delta\delta = \sum_j \Delta\delta_j \tag{5.1}$$

2. Integral layer coefficients $a_1, ..., a_4$ are calculated from $\alpha_1, ..., \alpha_4$.

3. Fluxes are calculated using the adding method, taking the integral layer coefficients as an input.

   Longwave: The adding method is performed in total five times with different choices of 'idealised' optical thickess, i.e. thickness assuming radiation exchanged with the surface, space, or neighouring layers (resp.).

5.2 Broadband Regions

The ACRANEB scheme operates in two spectral regions:

- Shortwave: 245 nm – 4.642 ▫m
- Longwave: 4.642 ▫m – 105.000 ▫m

In the shortwave region, there is a single source of radiation (the Sun, resp. Moon), which undergoes scattering and absorption in every layer.

In the longwave region, the surface and every layer is a source of radiation through thermal emission, but this complexity is somewhat reduced by the fact that scattering of infrared radiation by gases in the atmosphere is weak enough to be neglected, although scattering of infrared radiation by clouds and aerosols still needs to be taken into account.

5.3 Gaseous Transmission

The radiation model depends on the ability to calculate gaseous transmission function between arbitrary layers. Transmission functions are approximated by a *modified Malkmus model*. The complex absorption structure of a gas is parametrised by a small number of parameters as it is in the classical narrow-band Malkmus model, but in this case they describe the whole broadband region (shorwave or longwave). This greatly reduces the number of calculations needed to to compute a transmission function between two layers, but necessitate a range of compromises to be made.

5.3.1 Modified Malkmus Model

The modified Malkmus model is given by a heuristically derived formula based on the original Malkmus formula (Jan Mašek, Král, and Brožková 2012):

$$\tau_M = \frac{a}{2b}\left(\sqrt{1+\frac{4bu}{1-c/a}}-1\right) \tag{5.2}$$

$$\tau = \frac{\tau_0}{\alpha}\left[\left(1+\frac{\tau_M}{\tau_0}\right)^{\alpha}-1\right] \tag{5.3}$$

Coefficients a, b, and c depend on pressure and temperature by:

$$a = a_0(T/T_0)^{\alpha_a}, b = b_0(p_0/p)(T/T_0)^{\alpha_b}, c = c_0(p/p_0)(T/T_0)^{\alpha_c} \tag{5.4}$$

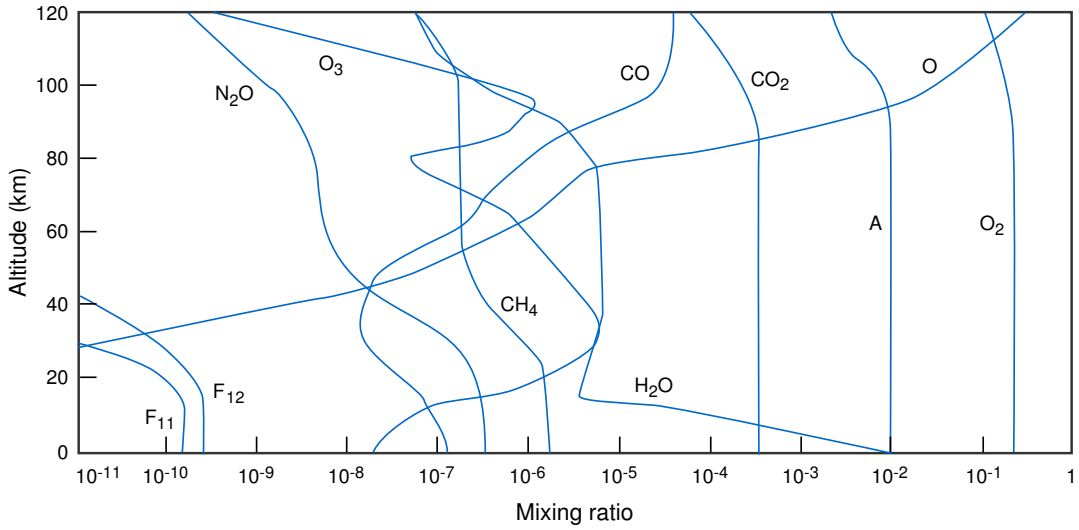

Figure 5.1: Atmospheric composition. Schematic figure showing concentration of some radiatively active gases in the atmosphere. Adapted from Goody and Yung 1989.

The parameters a_0, b_0, c_0, $\square_a$, $\square_b$, $\square_c$, $\square$ and $\square_0$ are determined by fitting the transmission function to a range of transmissions calculated by an external narrow-band model SPLIDACO.

5.3.2 Representation of Gases in ACRANEB

ACRANEB contain representation of all atmospheric gases which contribute significantly to the radiative energy budget in shortwave and longwave part of the spectrum:

- Water vapour
- O_3‘
- CO2+ (CO_2, CH_4, CO, N_2O, O_2)

CO_2, CH_4, CO, N_2O and O_2 are treated as a single *composite gas* (‘CO2+’), because they are well-mixed, and their concentration in the atmosphere is relatively constant[2] (Fig. **??**).

The absorption structure of each gas is described by a total of 16 parameters (8 for both parts of the spectrum), as detailed above.

[2]This is not neccessrily true for all conditions, because some of these gases have sources near the surface, e.g. CO_2 is released by vegetation and exhibits both spatial and seasonal variability. Nevertheless, this simplification is justified, because the impact on atmospheric heating rate is low [citation?].

5.4 Solving the RTE

The solution for broadband flux densities at layer interfaces is found by multiple passes of the adding method outlined in the previous chapter. The adding method allows for only single absorption and scattering coefficient to be specified per layer. While this is sufficient for monochromatic calculations when the absorption and scattering coefficients are independent from the flux density, in broadband calculations the power distribution of the flux needs to be taken into account. This is however not possible when fluxes combine contributions from multiple sources, with radiation having traversed different paths through the atmosphere.

One solution to the problem would be to carry out the adding method for every radiation source independently, and summing up the resulting fluxes (which can be done thank to linearity of the RTE). The power distribution of a broadband flux at a layer interface can then be known, because it is determined by the power distribution of the emitting source and the extinction along the path between the source and the layer. To be precise, the path traversed by radiation between the source and the layer is not known with full accuracy, because apart from the direct path, a fraction of the radiation can be scattered multiple times, taking a longer path before arriving at the layer.

While the method outlined above is feasible and relatively accurate, it is too computationally demanding to be performed at every time step, because the adding method would have to be repeated for each layer in the thermal spectrum (every layer is a source of radiation). The number of passes can be reduced when we consider the net exchange rate formulation:

i.e. when we compute the flux divergence R_k by the adding method, it is equal to the sum of CTS, EWS and EBL terms. For a suitable choice of sources,

5.5 Longwave Solution

In the longwave part of of the spectrum, there are many sources of radiation: the Earth's surface and each atmospheric layer. This fact makes the situation more complicated than in the shortwave part of the spectrum, as broadband optical thickness of layers depends on the path travelled by radiation, which is ambiguous. The adding method can accomodate only a single choice of optical thickness per layer. However, it is possible to overcome this problem with improved accuracy (over making a single arbitrary choice of optical thickness) by repeating the adding method with different choices of optical thickness and combining the results.

Firstly, we should observe that most of the radiation is exchanged with space by cooling to space (CTS). Second to that, significant amount of radiation is exchanged with surface (EWS). In the third place, radiation is exchanged between neighbouring layers and layers further away (EBL).

5.5.1 Simple Net Exchange Rate Formulation

Consider the following combination of fluxes obtained by the adding method with different choices of optical thickness and temperature profile:

$$\mathbf{F} = \mathbf{F}_0 + (\mathbf{F}_{\mathsf{CTS}} - \mathbf{F}_{0,\mathsf{CTS}}) + (\mathbf{F}_{\mathsf{EWS}} - \mathbf{F}_{0,\mathsf{EWS}}) \tag{5.5}$$

where $\mathbf{F}$ is a vector of fluxes at all layer interfaces, and:

- $\mathbf{F}_0$ is a vector of fluxes for the real temperature profile and optical thickness of each layer chosen to be the minimum of optical thickness as viewed from space and optical thickness as viewed the surface, i.e. $\tau_i = \min(\tau_{i,\mathsf{surface}}, \tau_{i,\mathsf{space}})$.
- $\mathbf{F}_{\mathsf{CTS}}$ is obtained from $\mathbf{F}'_{\mathsf{CTS}}$, which is a vector of fluxes for a temperature profile in which the surface and all layers have unit temperature and space has temperature of 0 K. Optical thickness of layers is chosen as viewed from space. $\mathbf{F}_{\mathsf{CTS}}$ is calculated from $\mathbf{F}'_{\mathsf{CTS}}$ in such a way that fluxes are turned into NER exchanges, each multiplied by the real thermal emission (σT^4) of the respective layer, and turned back into fluxes.
- $\mathbf{F}_{\mathsf{EWS}}$ is obtained from $\mathbf{F}'_{\mathsf{EWS}}$, which is a vector of fluxes for a temperature profile in which all layers and space have temperature of 0 K and surface has temperature of unity. Optical thickness of layers is chosen as viewed from the surface. $\mathbf{F}_{\mathsf{EWS}}$ is calculated from $\mathbf{F}'_{\mathsf{EWS}}$ in such a way that fluxes are turned into NER exchanges, each multiplied by the real thermal emission (σT^4) of the respective layer, and turned back into fluxes.
- $\mathbf{F}_{0,\mathsf{CTS}}$ is obtained from $\mathbf{F}'_{0,\mathsf{CTS}}$, which is a vector of fluxes for a temperature profile as in $\mathbf{F}_{\mathsf{CTS}}$ and optical thickness as in $\mathbf{F}_0$. $\mathbf{F}_{0,\mathsf{CTS}}$ is calculated from $\mathbf{F}'_{0,\mathsf{CTS}}$ by multiplying exchanges by real emission of layers as in $\mathbf{F}_{\mathsf{CTS}}$.
- $\mathbf{F}_{0,\mathsf{EWS}}$ is obtained from $\mathbf{F}_{0,\mathsf{EWS}}$, which is a vector of fluxes for a temperature profile as in $\mathbf{F}_{\mathsf{EWS}}$ and optical thickness as in $\mathbf{F}_0$. $\mathbf{F}_{0,\mathsf{EWS}}$ is calculated from $\mathbf{F}'_{0,\mathsf{EWS}}$ by multiplying exchanges by real emission of layers as in $\mathbf{F}_{\mathsf{EWS}}$.

Here, we used the 1:1 correspondence between the flux and NER representations. This seemingly complicated combination has a simple purpose: to remove CTS and EWS exchanges from $\mathbf{F}_0$ and replace them with CTS and EBW exchanges calculated with a more suitable choice of optical thickness. $\mathbf{F}_{0,\mathsf{CTS}}$ and $\mathbf{F}_{0,\mathsf{EWS}}$ are the terms which remove the CTS and EWS exchanges from $\mathbf{F}_0$, and $\mathbf{F}_{\mathsf{CTS}}$ and $\mathbf{F}_{\mathsf{EWS}}$ are the 'replacements' with the more suitable choices of optical thickness.

The 'simple' formulation described here was used in a previous version of ACRANEB, and has been superseded by an extended formulation with a greater accuracy (see below). The choice of $\tau_i = \min(\tau_{i,\text{surface}}, \tau_{i,\text{space}})$ in $\mathbf{F}_0$ is pragmatic: it minimises exchanges between layers, which is assumed to lead to a better model stability (J. Mašek, personal communication, November 13, 2013).

5.5.2 Net Exchange Rate Formulation with 'Bracketing'

The formulation outlined in the previous section still does not represent exchanges between layers accurately. Especially, optical thickness used in the calculation of $\mathbf{F}_0$ is an extreme case. An improved formulation takes into the account the fact that optical thickness in EBL (exchange between layers) terms should be between two extreme values:

$$\mathbf{F} = (1-\alpha)(\mathbf{F}_1 - \mathbf{F}_{1,\text{CTS}} - \mathbf{F}_{1,\text{EWS}}) + \alpha(\mathbf{F}_2 - \mathbf{F}_{2,\text{CTS}} - \mathbf{F}_{2,\text{EWS}}) + \tag{5.6}$$

$$+ \mathbf{F}_{\text{CTS}} + \mathbf{F}_{\text{EWS}} \tag{5.7}$$

where:

- $\mathbf{F}_1$ is a vector of fluxes for the real temperature profile and optical thickness of each layer chosen to be the *minimum* of optical thickness as viewed from space and optical thickness as viewed the surface, i.e. $\tau_i = \min(\tau_{i,\text{surface}}, \tau_{i,\text{space}})$.
- $\mathbf{F}_2$ is a vector of fluxes for the real temperature profile and optical thickness of each layer chosen to be the *maximum* of optical thickness as viewed from space and optical thickness as viewed the surface, i.e. $\tau_i = \max(\tau_{i,\text{surface}}, \tau_{i,\text{space}})$.
- $\mathbf{F}_{1,\text{CTS}}$ and $\mathbf{F}_{1,\text{EWS}}$ are obtained in analogy to $\mathbf{F}_{0,\text{CTS}}$ and $\mathbf{F}_{0,\text{EWS}}$ (resp.) of the 'simple' NER formulation, but with optical thickness as in $\mathbf{F}_1$.
- $\mathbf{F}_{2,\text{CTS}}$ and $\mathbf{F}_{2,\text{EWS}}$ are obtained in analogy to $\mathbf{F}_{0,\text{CTS}}$ and $\mathbf{F}_{0,\text{EWS}}$ (resp.) of the 'simple' NER formulation, but with optical thickness as in $\mathbf{F}_2$.
- $\mathbf{F}_{\text{CTS}}$ and $\mathbf{F}_{\text{EWS}}$ are the same as in the 'simple' NER formulation.

The idea behind this complicated formulation is that $\mathbf{F}_{1,\text{CTS}}$ and $\mathbf{F}_{1,\text{EWS}}$ remove CTS and EWS exchanges from $\mathbf{F}_1$, $\mathbf{F}_{2,\text{CTS}}$ and $\mathbf{F}_{2,\text{EWS}}$ remove CTS and EWS exchanges from $\mathbf{F}_2$, their linear combination is taken according to a real parameter α, and CTS and EWS exchanges are supplied by $\mathbf{F}_{\text{CTS}}$ and $\mathbf{F}_{\text{EWS}}$.

5.6 Net Exchange Rate Formulation

The adding method introduced in the previous chapter can be used to calculate fluxes at layer interfaces when source terms (sources of radiation) and optical depths of layers are known. However, this approach cannot be used directly for broadband calculations. This is because the optical depths are dependent on the actual power distribution with wavelength in affected flux, i.e. certain wavelengths can be selectively depleted by previous absorption, and further absorption becomes saturated (non-linear). Because there is only one broadband flux incorporation contributions of many sources, there is no way of specifying single right optical depth of a layer in the adding method equation. But this does not preclude the possibility to find one that is the most optimal.

An important observation about the radiative transfer problems is that it is linear – the radiative transfer equation can be solved separately for each radiation source, and total radiances (or fluxes) can be obtained by summing the elemental solutions. Therefore, in theory, the adding method can be applied for each radiation source only, ensuring that layer optical depths can be chosen (almost) unequivocally, because the path between the layer and source is well known. The only exception is multiple scattering, when the path is prolonged, but this may be a relatively negligible effect. This method however cannot be femployed efficiently in radiative transfer models, because there are too many sources (in the longwave spectrum every layer is a source). But some sources are more important than others – radiation exchange with surface and space are generally stronger than exchanges between layers. The space is not a radiation source (rather a 'sink'), but the situation can be mathematically inverted to treat it as a source instead.

ACRANEB, being a broadband radiative model, has to make a number of simplifying assumptions in order to be able to leverage the adding method.

5.6.1 Statistical Model

5.6.2 Autoevaluation

5.7 Verification

ACRANEB belongs to the category of less accurate but fast radiative transfer models. As such, it can use RRTM or LBL models as a verification target.

Chapter 6

Shortwave Intermittency in ACRANEB2

As the atmospheric gaseous composition and temperature and pressure profile do not change as quickly as the cloud cover, we can speed up radiative computations by calculating gaseous optical thicknesses less frequently than the rest of the variables. In other words, we can introduce an *intermittence* period longer than the model time step during which the gaseous optical thicknesses are not recalculated.

In the thermal part of the spectrum, we can achieve this by simply maintaining constant optical thicknesses during the intermittence period. In the solar spectrum, however, the situation is complicated by the fact that optical thickness depends on the zenith angle. It is therefore necessary to devise a method of accounting for this change without the need to do a full recalculation of optical thicknesses.

This chapter discusses design, implementation and evaluation of shortwave intermittence in the context of a single cell model and the NWP model ALADIN/ALARO.

6.1 Theoretical Considerations

In the following text, we assume a broadband model with two bands (solar and thermal), plane-parallel and delta-two stream approximations.

6.1.1 Monochromatic light

Let us first consider the simple case of monochromatic light passing through a homogeneous atmospheric layer. Radiation passing at cosine of the zenith angle μ is attenuated exponentially by the Beer-Lambert law:

$$I(z_2) = I(z_1) \exp\left(-\frac{1}{\mu} k \Delta u\right) \tag{6.1}$$

where k is the mass extinction coefficient, and Δu is the mass of the absorber per unit area. Here, $\frac{1}{\mu}k\Delta u$ is the *optical path* through the layer.

In addition to *optical depth*, we use the concept of *optical thickness*. The *optical thickness* of a layer is commonly defined as the optical path through the layer in the vertical direction ($\mu = 1$), but we note that this is the same as normalizing the actual optical path by μ:

$$\tau := \tau(z_1, z_2; \mu = 1) = k\Delta u = \mu \left(\frac{1}{\mu} k\Delta u \right) = \mu\tau(z_1, z_2; \mu) \tag{6.2}$$

where $\tau(z_1, z_2; \mu)$ denotes optical path for radiation passing at the (cosine of) angle μ. We use the same symbol τ for optical thickness and optical depth, but stating its meaning explicitly where needed. In the monochromatic case, both definitions are equivalent, but the latter generalizes better to the broadband radiation treatment, where the Beer-Lambert law no longer holds. We will therefore use this latter definition:

$$\tau := \mu\tau(z_1, z_2; \mu) \tag{6.3}$$

6.1.2 Downward and upward broadband optical thickness

In a broadband radiative transfer scheme, it is necessary to distinguish downward and upward optical thickness of a layer. This is because the optical thickness depends not only on the properties of the layer (as in monochromatic case), but also the spectral composition of the radiation entering the layer and the length of the path through the layer, which determines the amount of spectral saturation.

The downward solar optical thickness is calculated for parallel radiation coming directly from the Sun at a zenith angle θ and is equal to the optical path through the layer normalized by cosine of the zenith angle (which is proportional to the length of the path).

The upward solar optical thickness, on the contrary, is calculated for diffuse radiation reflected from the surface, which does not have any associated direction in the δ-two stream approximation. In this case, the dependence on the zenith angle is only through its influence on the spectrum of the incoming radiation, which has passed through the atmosphere as parallel radiation at the given zenith angle.

The geometry of the downward case is depicted in Fig. 6.1.

6.1.3 Modified cosine of the zenith angle

The actual angle at which radiation passes through an atmospheric layer is not the same as the zenith angle. This is due to the sphericity of the atmosphere, and is particularly

true for high zenith angles ($\mu \to 0$).

In order to transparently account for this effect, the ACRANEB2 scheme uses a modified cosine of the zenith angle in place of μ (J Mašek et al. 2014):

$$\mu' = \frac{1}{\left(\left(\frac{a}{H}\mu\right)^2 + 2\frac{a}{H} + 1\right)^{1/2} - \frac{a}{H}\mu} \tag{6.4}$$

where a is the radius of the Earth, and H is the approximate height of the atmosphere. The ratio H/a was chosen to be a constant of 0.001324, for which $\mu'(\mu = 0) = 38.88$[1]. This has an additional benefit of preventing $1/\mu$ growing to infinity as $\mu \to 0$ in numerical calculations.

The modified cosine of the zenith angle is the natural coordiate for studying the change of optical thickness with the position of the Sun in the sky.

6.2 Analysis Using a Single Column Model

In order to empirically investigate dependece of broadband gaseous optical thicknesses on the zenith angle, we can use a single column model to calculate optical thicknesses for varying values of the zenith angle. We used multiple runs of the ACRANEB2 SCM model over a range of μ values from the interval $[0, 1]$.

6.2.1 Dependece of optical thickness on the zenith angle

The plot in Fig. 6.2 shows the result for a clear sky atmosphere with 87 layers in standard and log-log coordinates. The dependence is plotted as a function of the modified cosine of the zenith angle (see above). As you can see from the logarithmic plot, the dependence is close to a power function (i.e. is linear in the logarithmic coordinates). This suggest that a linear interpolation between extreme values of the zenith angle in an intermittence period could yield accurate enough results. Similar relatiotionship was observed in cloudy atmosphere and a number of additional cases.

6.2.2 Linear interpolation of optical thicknesses

As justified by the empirical analysis of optical thickness dependence on the zenith angle, we performed an experiment with the single column model where the log optical thicknesses were linearly interpolated with respect to log of the modified cosine of the

[1] It should be noted that the true angle at which radiation passes through a layer depends on the layer height, but here an independent scaling was used. It is also affected by refraction, which is omitted as well.

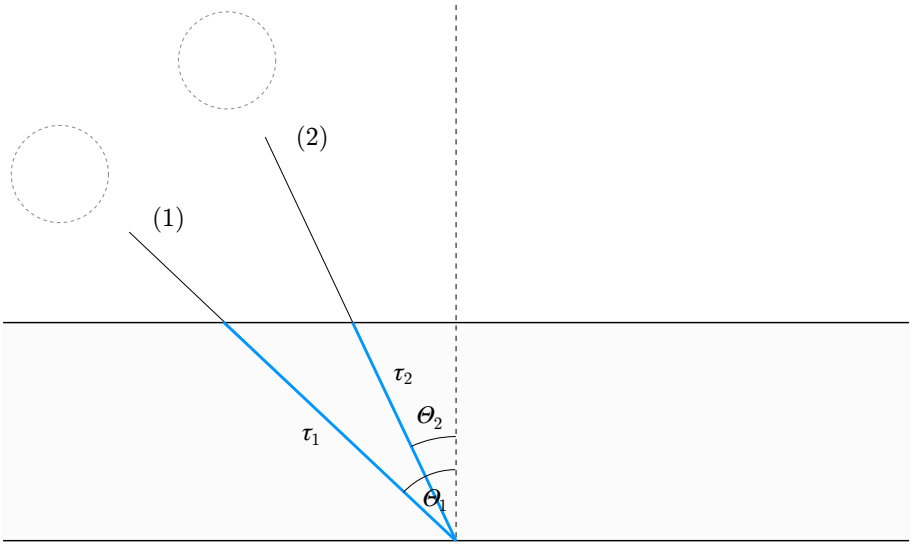

Figure 6.1: Geometry of the shortwave intermittency problem (downward). (1) At the beginning of the intermittence period, solar radiation passes through a plane-parallel atmospheric layer at zenith angle θ_1. (2) As the Sun rises to zenith angle θ_2, the broadband optical thickness (as per our definition) of the layer changes from τ_1 to τ_2. Note that $\tau_2 > \tau_1$, as the broadband optical thickness equals to optical path normalized by $\mu = cos(\theta)$, which is proportional to the length of the path.

zenith angle. The Fig. 6.3 shows the result for a clear-sky atmosphere, and a choice of shortwave intermittency interval of $\Delta\theta = 15°$ (1 h on the equator on equinox). The heating rates were compared to the reference (non-interpolated) case. The difference in heating rates was the most significant for high zenith angles (low $\cos(\mu)$), when the change in the zenith angle corresponds to a large change in the cosine of the zenith angle. The difference was within 0.1 K/day (5 %) for all but the top layers, which is an acceptable loss of accuracy compared to the rest of the broadband radiative scheme.

6.2.3 More cases

We performed the same analysis as above on multiple other cases: a *cloudy atmosphere* with the same temperature and composition profiles, *tropical*, *midlatitude summer* and *winter* atmospheres, and *subarctic summer* and *winter* atmospheres[2]. The cloudy atmosphere did not differ significantly from the clear sky case. The tropical, midlatitude and subarctic cases had error of the heating rate within 0.5 K/day.

[2]Plots of all studied cases can be found in the Additional Materials (see the end of this report).

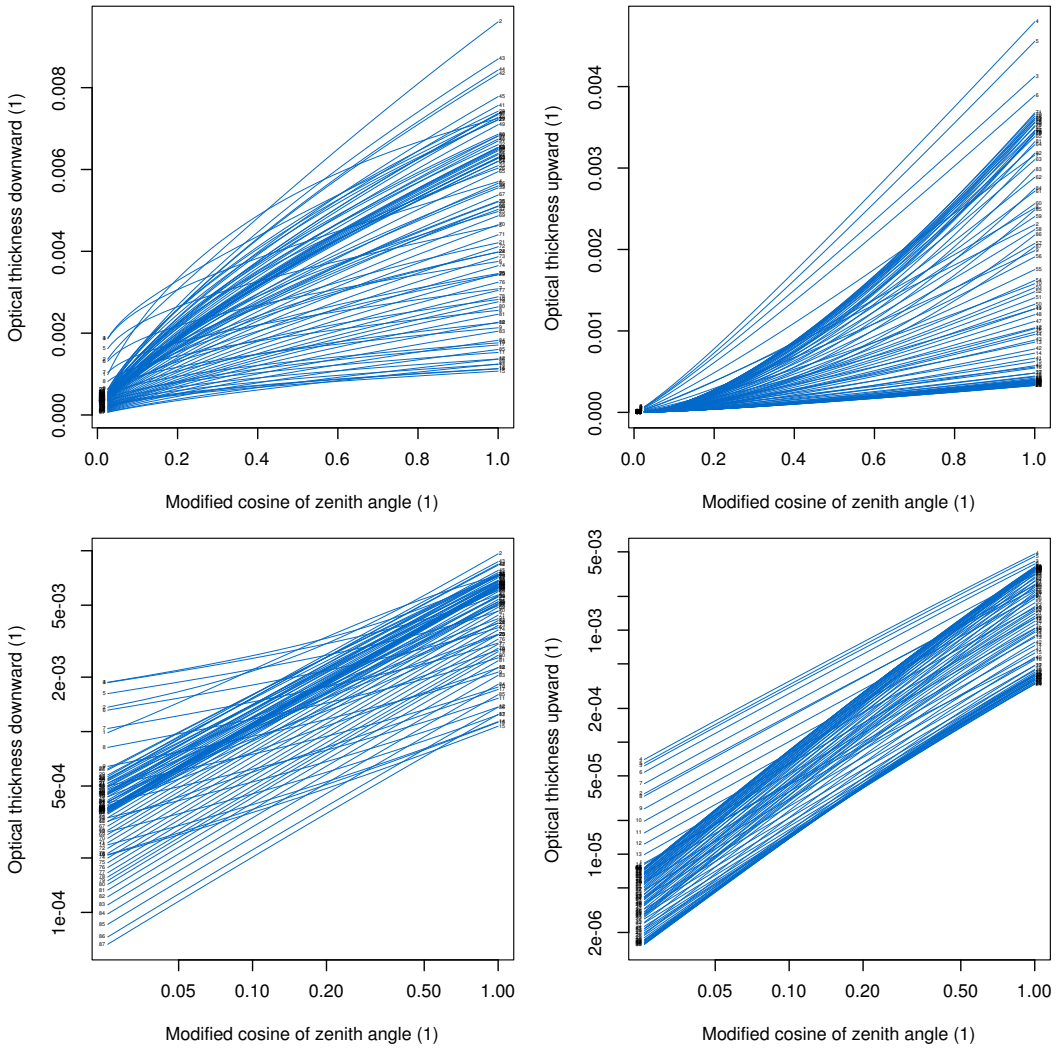

Figure 6.2: Optical thickness of layers as a function of the modified cosine of the zenith angle. Downward optical thickness in ordinary (**top-left**) and log-log coordinates (**bottom-left**), and upward optical thickness in ordinary (**top-right**) and log-log coordinates (**bottom-right**). Lines are labeled with layer numbers. Note that the relationship is almost linear in the log-log coordinates.

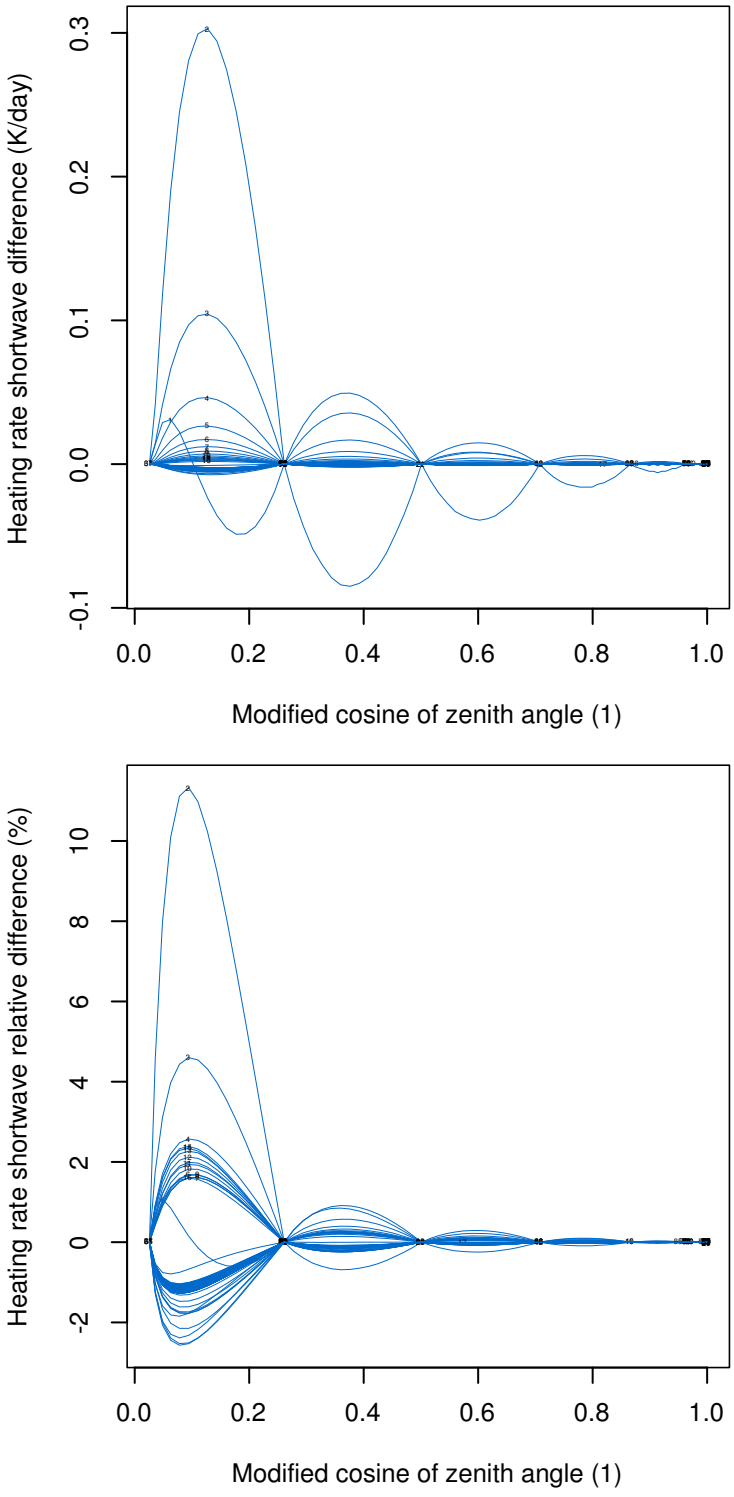

Figure 6.3: Heating rate difference between the reference and linearly interpolated optical thicknesses at 15° steps of the zenith angle. Plots show absolute difference in heating rate (**top**), and relative difference in heating rate in per cent (**bottom**).

6.3 shortwave intermittency Implementetion in a 3D Model

The results from the Single Colomn Model support the application of shortwave intermittency in a 3-dimensional NWP model. This was implemented in the ACRANEB2 scheme in the ALADIN/ALARO[3] model.

In the 3D model, the radiative transfer scheme calculates radiative transfer independently for each grid point of the model domain.

6.3.1 Overview of the implementation

At the beginning of an intermittence period (*full* radiative time step):

1. Calculate the mimimum and maximum values of the zenith angle attained at any time step during the intermittence period. Store the zenith angles (the extreme values as well as the values at all time steps) in global arrays (preserved across time steps).
2. Calculate solar optical thicknesses as usual for the two extreme values the zenith angle. Store (the logarithm of) the optical thicknesses in global arrays.

At every time step *within* the intermittence period (*partial* radiative time step):

1. Retrieve current zenith angle from the global array (ignoring the zenith angle supplied by the model), and continue all computations with this zenith angle.
2. Calculate optical thicknesses by interpolating between the extreme optical thicknesses as stored in the global arrays.

6.3.2 Technical considerations

There were a number of additional technical considerations which needed to be taken into account when implementing shortwave intermittency in a 3D model:

1. **Solar declination.** Solar declination varies during the intermittence period. In our case, the model does no provide the scheme with solar declination for the subsequent time steps, nor a straighforward way of calculating it[4]. In order to simplify implementation, solar declination within intermittency period is kept constant. This is justified since the length of the intermittency period is not expected to be chosen long enough for the variation of solar declination to be important.

[3] ALARO cycle 38.
[4] Without copying a significat amount of code.

2. **Storage requirements.** Shortwave intermittency requires us to store fields of downward and upward optical thickness at two extreme values of the zenith angle. This results in four 3D global fields of optical thickness and a number of 2D global fields of zenith angles to be kept in the main memory between time steps.

3. **Day/night segmentation.** The ACRANEB2 scheme performs calculations on blocks of grid points in a vectorizable form[5]. The solar computations are only performed on segments of grid points where the Sun is in the sky. This selection has to be extended with grid points where the zenith angle is positive at any time during the intermittence period.

4. **Modularization.** The shortwave intermittency implementation required more modularization in terms of decoupling the solar and thermal computations of optical thickness.

6.4 Analysis

In order to evaluate accuracy and performance of the implementation of shortwave intermittency, we performed a number of simulations (experiments) with the ALADIN/ALARO NWP model and analysed the results.

6.4.1 Analysis Description

The simulations were performed on a domain covering Central Europe. Values for offline analysis were sampled from a limited number of points chosen evenly from the whole domain (Figure 6.4). A 24-h summer day convective situation starting at 0:00 UTC, 29 May 2009 was chosen for the analysis.

For the purpose of gathering data from the selected points during model run, tools called nc_dump[6] and dump2h5[7] were developed. These made it possible to export fields into NetCDF/HDF5 files, which were subsequently analysed using a set of short programs made in the statistical programming language R. The entire analysis is available openly at https://github.com/peterkuma/acraneb2-intermittency-analysis.

6.4.2 Experiments

The following experiments were performed:

[5] In the sense of performing an operation on a sequence of values simultaneously by a single processor (on processors which support such a feature).

[6] https://github.com/peterkuma/nc_dump

[7] https://github.com/peterkuma/dump2h5

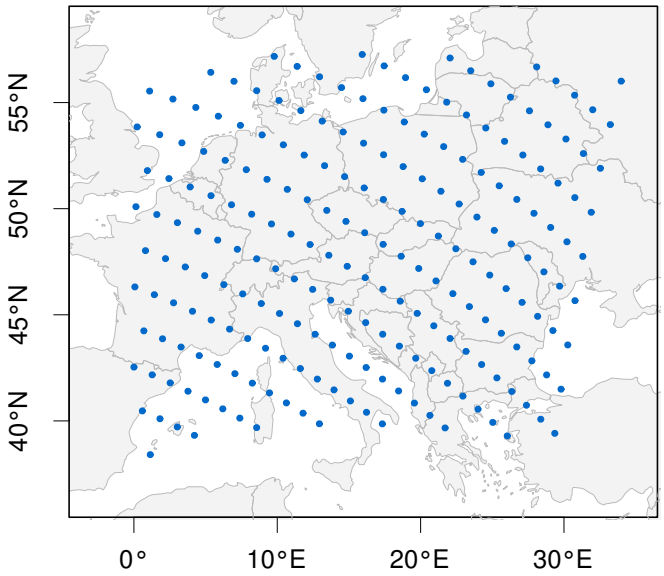

Figure 6.4: Points on the model domain sampled for offline analysis. Data from the points shown were saved during model runs for later (offline) analysis at every time step of the simulation.

1. **Shortwave Intermittency Base**

   Base configuration for shortwave intermittency evaluation:

   - Shortwave gaseous transmissivities computed at every time step.
   - Longwave gaseous transmissivities computed once per 1 h.
   - Calibration of longwave NER weights computed once per 3 h.

2. **Shortwave Intermittency 1 h**

   Shortwave intermittency enabled with 1 h intermittency:

   - Based on *Shortwave Intermittency Base*.
   - Shortwave gaseous transmissivities computed once per 1 h.

6.4.3 Accuracy

In order to determine how the shortwave intermittency affects accuracy, we looked at the global bias of heating rates, as well as the local error and its statistical distribution. Figure 6.5 shows the error in heating rate of 1 h shortwave intermittency compared to no shortwave intermittency (Exp. *Shortwave Intermittency 1 h* vs. Exp. *Shortwave Intermittency Base*). The local error was less than 0.2 K/day in 95 % of samples, and the global error was on the order of 0.01 K/day.

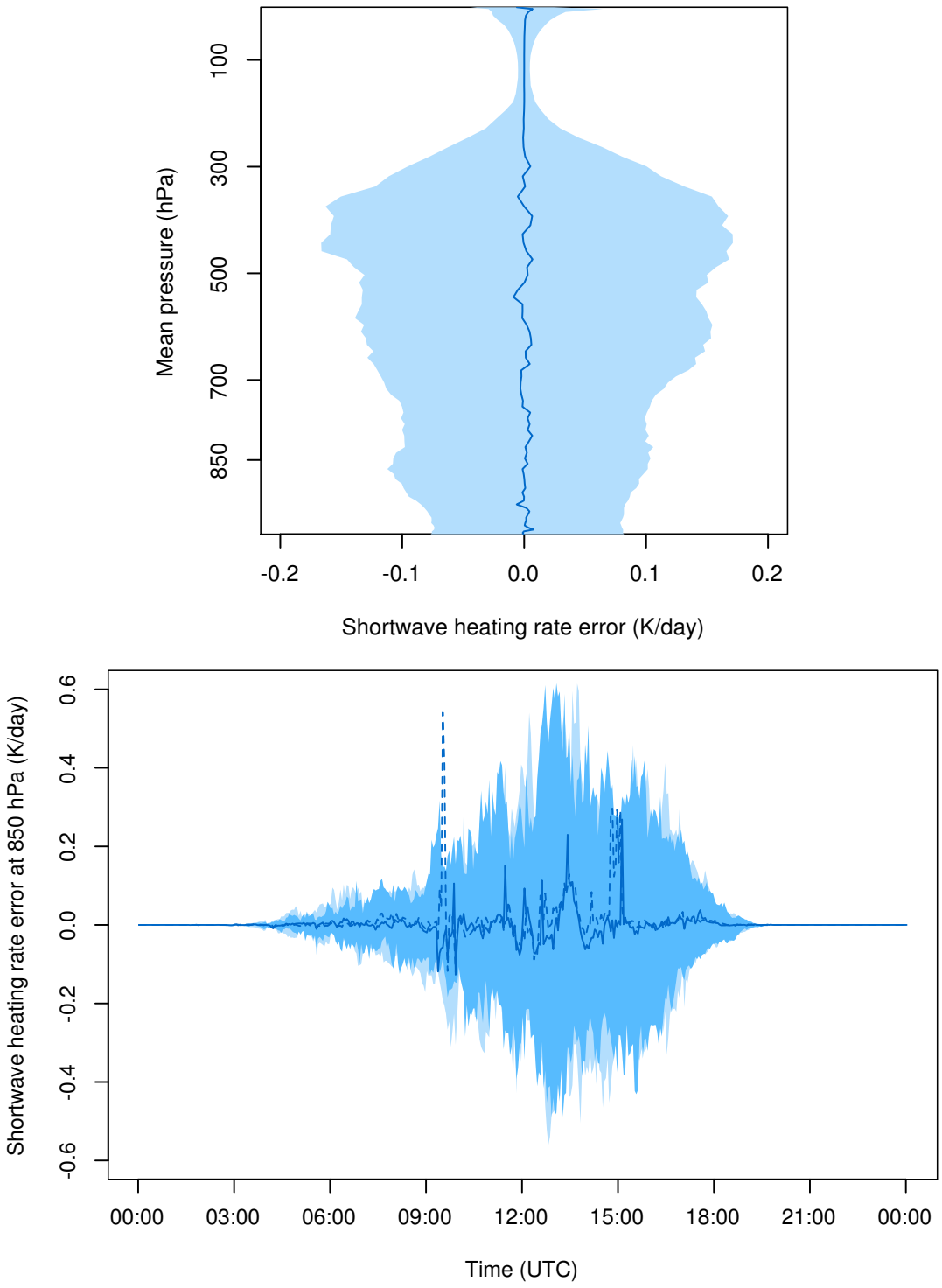

Figure 6.5: Shortwave heating rate error of 1 h shortwave intermittency. Shown is a global bias (**top**) and time series (**bottom**) of heating rate and 95 % confidence bands of a model run with 1 h shortwave intermittency compared to no shortwave intermittency. The situation is a convective summer day of 29 May 2009 over Central Europe.

Table 6.1: Impact of solar intermittency on the model computation time. The table lists full NWP model computation time of 6-hour integration, 180-s time step (case 2012-07-01T00:00:00Z) for a number of different configurations. Time is expressed relative to the baseline case. *Note:* Memory increase due to solar intermittency was 2.4 %.

Day/night computation	Solar intermittency	Time (relative)
Yes	No	1.00
No	No	1.02
No	Yes, 0 h	1.08
No	Yes, 1 h	1.04
Yes	Yes, 0 h	1.05
Yes	Yes, 1 h	**0.95**

6.4.4 Performance

We measured performance of the new scheme using a 24-h run of the NWP model on 4 CPUs of a NEC SX-9 supercomputer (100 GFLOPS per CPU). The decrease in total model computation time with 2-h shortwave intermittency was 5 %, which is in our experience a significant reduction. See Tab. 6.1 for details.

6.5 Conclusion

shortwave intermittency is a viable approximation in plane-parallel broadband radiative transfer schemes. By avoiding calculation of solar gaseous optical thicknesses at every time step we gain a signification reduction in computation time, while maintaining good accuracy of heating rates.

Linear interpolation of optical thickness on logarithic scale is enough to account for the dependence of optical thickness on the relatively quickly-changing zenith angle for intermittence periods up to 2 hours long (at least).

6.6 Additional Materials

All additional materials used in the analysis can be found at https://github.com/peterkuma/solar-intermittence.

The ACRANEB2 single column model and changes to the code cannot be made publicly available as they are proprietary.

Chapter 7

Longwave Intermittency in ACRANEB2

Chapter 8

Conclusion

Appendix A

ACRANEB2 Configuration Parameters

This appendix documents some of the configuration parameters used in the ACRANEB2 radiation scheme, esp. those relevant to computational intermittency. The parameters are set as variables in a Fortran namelist supplied to the SCM (single column model) or the NWP model ALARO. More configuration parameters are documented briefly in `Arp/module/yomphy.F90` in the ALADIN/ALARO source code.

A.1 Intermittency Parameters

A.1.1 NSORAYFR

`NSORAYFR=<n>`
`NSORAYFR=-<h>`

Shortwave (solar) intermittency interval length. Shortwave gaseus transmissivities are calculated every `<n>` steps, resp. every `<h>` hours.

A.1.2 NRAUTOEV

`NRAUTOEV=<n>`

Intermittency interval of calculation of NER 'bracketing' weights in the thermal (longwave) computation. Weights are calculated every `<n>` full radiation steps, or disabled when `<n>` = 0.

A.1.3 LRAYPL

`LRAYPL=.T.|.F.`

Turn on or off day/night slicing of grid blocks. If enabled, shortwave computation is restricted to 'day' grid cells, possibly improving performance.

A.1.4 NTHRAYFR

`NTHRAYFR=<n>`
`NTHRAYFR=-<h>`

Longwave (thermal) intermittency interval length. Longwave gaseous transmissivities are calculated every `<n>` steps, resp. every `<h>` hours.

Bibliography

Geleyn, JF, R Fournier, et al. (2005). "A new 'bracketing' technique for a flexible and economical computation of thermal radiative fluxes, scattering effects included, on the basis the Net Exchanged Rate (NER) formalism". In: *Research Activities in Atmospheric and Oceanic Modelling (Blue Book)*. WMO: CAS/JSC Working Group on Numerical Experimentation. URL: http://www.wcrp-climate.org/WGNE/BlueBook/2005/chapters/04.pdf.

Geleyn, JF and A Hollingsworth (Feb. 1979). "An Economical Analytical Method of the Computation of the Interaction Between Scattering and Line Absorption of Radiation". In: 50.1.

Goody, Richard M and Yuk Ling Yung (1989). *Atmospheric Radiation: Theoretical Basis*. Oxford University Press.

– (1995). *Atmospheric Radiation: Theoretical Basis*. Oxford University Press. ISBN: 978-0195102918.

Liou, Kuo-Nan (2002). *An Introduction to Atmospheric Radiation, Second Edition*. Vol. 84. Academic Press. ISBN: 978-0124514515.

Mašek, Jan, Tomáš Král, and Radmila Brožková (2012). *Rehearsal of the gaseous transmission functions*. URL: http://www.rclace.eu/File/ALARO/alaro1_wd12lj/alaro1wd_JM_radiation_jun12.pdf.

Mašek, J et al. (2014). "Single interval shortwave radiation scheme with parameterized optical saturation and spectral overlaps". In: Manuscript submitted for publication.

Mlawer, Eli J et al. (2012). "Development and recent evaluation of the MT_CKD model of continuum absorption". In: *Philosophical Transactions of the Royal Society A: Mathematical, Physical and Engineering Sciences* 370.1968, pp. 2520–2556.

Petty, Grant W. (2006). *A First Course in Atmospheric Radiation, Second Edition*. Sundog Publishing. ISBN: 978-0-9729033-1-8.

Ritter, Bodo and Jean-Francois Geleyn (1992). "A comprehensive radiation scheme for numerical weather prediction models with potential applications in climate simulations". In: *Monthly Weather Review* 120.2, pp. 303–325.

Serdyuchenko, A et al. (2013). "High spectral resolution ozone absorption cross-sections–Part 1: Measurements, data analysis and comparison with previous measurements around 293 K". In: *Atmospheric Measurement Techniques Discussions* 6.4. Data: http://igaco-o3.fmi.fi/ACSO/files/cross_sections/

Serdyuchenko / SerdyuchenkoGorshelev5digits . dat, pp. 6567–6611. URL: http://www.atmos-meas-tech-discuss.net/6/6567/2013/amtd-6-6567-2013.pdf.

Solomon, S et al. (1998). "Absorption of solar radiation by water vapor, oxygen, and related collision pairs in the Earth's atmosphere". In: *Journal of Geophysical Research: Atmospheres (1984–2012)* 103.D4, pp. 3847–3858.

Zdunkowski, Wilford, Thomas Trautmann, and Andreas Bott (2007). *Radiation in the Atmosphere: A Course in Theoretical Meteorology*. Cambridge University Press. ISBN: 978-0-521-87107-5.